Optimizing Four Years of CO_2 Biospheric Fluxes from OCO-2 and in situ data in TM5 : Fire Emissions from GFED and Inferred from MOPITT CO data

Hélène Peiro [1], Sean Crowell [1], and Berrien Moore III [1]

[1]University of Oklahoma, Norman, OK, USA

Correspondence: Helene Peiro (helene.peiro@ou.edu)

Abstract. Column mixing ratio of carbon dioxide (CO_2) data alone do not provide enough information for source attribution. Carbon monoxide (CO) is a product of inefficient combustion often co-emitted with CO_2. CO data can then provide a powerful constraint on fire emissions, supporting more accurate estimation of biospheric CO_2 fluxes. In this framework and using the chemistry transport model TM5, a CO inversion using MOPITT v8 data is performed to estimate fire emissions which are then converted in CO_2 fire emissions (called FIREMo) through the use of emission ratio. These optimized CO_2 fire emissions (FIREMo) are used to re-balance the CO_2 Net Ecosystem Exchange (NEEmo) and respiration (Rmo) with the global CO_2 growth rate. Subsequently, in a second step, these rebalanced fluxes are used as priors for a CO_2 inversion to derive the NEE and ocean fluxes constrained either by the Orbiting Carbon Observatory 2 (OCO-2) v9 or by in situ CO_2 data. For comparison purpose, we also balanced the respiration using fire emissions from the Global Fire Database Emissions (GFED) version 3 (GFED3) and version 4.1s (GFED4.1s). We hence study the impact of CO fire emissions in our CO_2 inversions at global, latitudinal and regional scales over the period 2015 - 2018 and compare our results to the two other similar approaches using GFED3 (FIRE3) and GFED4.1s (FIRE4) fires, as well as with an inversion using both CASA-GFED3 NEE and GFED3 fire priors (priorCMS). After comparison at the different scales, the inversions are evaluated against TCCON data. Comparison of the flux estimates show that at global scale posterior net flux estimates are more robust than the different prior flux estimates. However, at regional scale, we can observe differences in fire emissions among the priors, resulting in large adjustments in the NEE to match the fires and observations. Tropical flux estimates from in situ inversions are highly sensitive to the prior flux assumed, of which fires are a significant component. Slightly larger net CO_2 sources are derived with posterior fire emissions using either FIRE4 or FIREMo in the OCO-2 inversion, in particular for most Tropical regions during 2015 El Nino year. Similarly, larger net CO_2 sources are also derived with posterior fire emissions in the in-situ data inversion for Tropical Asia. Evaluation with TCCON data shows lower biases with the three re-balanced priors than with the prior using CASA-GFED3. However, posteriors have average bias and scatter very close each other, making it difficult to conclude which simulation is better than the other. One major conclusion from this work is the strong constrain at global scale of the data assimilated compared to the fire prior used. But results in the tropical regions suggest sensitivity to the fire prior for both the IS and OCO-2 inversions. Further work is needed to improve prior fluxes in tropical regions where fires are a significant component. Finally, even if the inversions using the FIREMO prior did enhance the biases over some TCCON sites, it is not the case for

the globe. This study consequently push forward the development of a CO-CO_2 joint inversion with multi-observations for possible stronger constraint in posterior CO_2 fire and biospheric emissions. Further work is needed to improve prior fluxes in Tropical regions where fires are a significant component.

1 Introduction

Carbon dioxide (CO_2) is the most important greenhouse gas contributing to global climate change (IPCC, 2014). Gaps in our understanding of the processes that control land-sea-atmosphere exchange of CO_2 are a leading order uncertainty in future projections of the global climate (Friedlingstein et al., 2014). The global net flux, and hence the airborne fraction, can be deduced from the atmospheric growth rate (Ballantyne et al., 2012), and historically different efforts, such as the Global Carbon Project (Le Quéré et al., 2009) have divided the total global net flux into its constituent components, consisting of fluxes from the ocean, terrestrial biosphere, fossil fuel combustion and other anthropogenic activities, and biomass burning.

CO_2 emissions from fires are well-characterized at the largest space and time scales, but the uncertainties increase rapidly as we look to finer space and time scales. Two approaches are currently employed to estimate global emissions from fires. The first uses, since 2017, total fuel consumption per product of the burned area and the fuel consumption per unit area deduced from the burned area and active fires products of the Moderate Resolution Imaging Spectroradiometer (MODIS). Previous years were based directly on burned area datasets. The Global Fire Emissions Database (GFED) products (van der Werf et al., 2010) and the Fire INventory from NCAR (FINN) (Wiedinmyer et al., 2011), for instance, use this approach. GFED was developed for understanding monthly contribution of fires to global carbon cycling (van der Werf et al., 2004), while FINN was developed for near real-time estimation (Wiedinmyer et al., 2011). The second technique deduces fuel consumption from Fire Radiative Power (FRP) determined from infrared thermal measurements. Two emission inventories use this approach, the Global Fire Assimilation System (GFAS) (Kaiser et al., 2012) and the Quick Fire Emissions Database (QFED) (Darmenov and Silva, 2015). Several studies used and compared these fire emissions inventories and found several differences in capturing wildfire activity over different areas as well as sources of uncertainties from the cloud gap adjustments, small fires estimations and land use and land cover estimation (Liu et al., 2020). While these fire emission inventories all use the MODIS thermal anomalies (Giglio et al., 2006), they use different methods of translating emission factors and land cover to estimate fire emissions. Although the quantification of emissions from biomass burning from space-based instruments has increased significantly, uncertainties regarding input data and methodologies can still lead to errors up to an order of magnitude for the total trace gases emissions (Vermote et al., 2009; Baldassarre et al., 2015).

Moving from global annual fluxes to finer scales in space and time complicates the inference a great deal. Interpreting atmospheric measurements of CO_2 at these scales requires the use of an atmospheric chemistry transport model (CTM) and assimilation system, frequently referred to in the literature as "atmospheric inversions", or "top-down inversions". However, even using the same set of observations such as the Orbiting Carbon Observatory 2 (OCO-2) data in different inverse modeling systems can induce a large range of CO_2 fluxes estimation at regional scales (Crowell et al., 2019; Peiro et al., 2022). Flux estimates from top-down inversions have been shown to be sensitive to the choice of transport model (Schuh et al., 2019), and

observational coverage (Byrne et al., 2017). Even more importantly, atmospheric measurements of CO_2 dry air mole fractions represent the combined influence of all upstream emissions and transport, and so individual tracer measurements cannot be used to differentiate between different source or sink processes without more information. Additionally, prior estimate of the fluxes and their associated uncertainties can impact posterior CO_2 estimations (Lauvaux et al., 2012b, a; Byrne et al., 2017; Gurney et al., 2003; Wang et al., 2018; Chevallier et al., 2005; Baker et al., 2006, 2010). A few studies (Liu et al., 2017a; Palmer et al., 2019; Crowell et al., 2019; Peiro et al., 2022) utilized XCO_2 from OCO-2 to constrain top-down surface fluxes of CO_2. All of the mentioned studies found the Tropics to be a large source region for 2015-2016, though the explanations varied. Crowell et al. (2019) showed that an ensemble of inversion models delivered robust results for Tropical regions when OCO-2 data was assimilated. The ensemble employed included different atmospheric transport models, prior ocean and terrestrial biosphere and fire fluxes, and assimilation techniques. All of the participating models did not optimize fire and fossil fuel emissions. As such, only the non-fossil land (net biosphere exchange; NBE) and ocean flux at regional scales was examined in the study, with no attempt to attribute ensemble spread to different sources of uncertainty, such as the assumed fire emissions, which neglected to include some of the global inventories, such as FINN, QFED, and GFED4.1s (earlier versions of GFED were included).

Most inversion models do not explicitly constrain fire emissions with CO_2 observations. Rather, it is assumed that fire emissions have much lower uncertainty (generally believed to be less than 10% (Quéré et al., 2018; Quilcaille et al., 2018)) than the ocean and terrestrial biosphere fluxes (Quéré et al., 2018; Khatiwala et al., 2009, 2013), and so are held fixed, with the net ecosystem exchange (NEE) being assumed to be the residual between the posterior total net land flux and the assumed fire and fossil fuel emissions. This inference is problematic, not least due to the aforementioned fire emissions uncertainties in time and space, which could alias into inferred biospheric fluxes at continental or regional scales (Wiedinmyer and Neff, 2007; Peylin et al., 2013). To reduce the uncertainties associated with fires and consequently with CO_2 biospheric emissions, we can examine gas species that are co-emitted with CO_2 from fires, such as carbon monoxide (CO).

CO is an air pollutant that affects the oxidation capacity of the atmosphere through its reaction with the hydroxyl radical (OH), leading to a relatively short atmospheric lifetime of one to three months because of its fast oxidation with OH. Reactions between CO and OH impact atmospheric composition on hemispheric (mainly in the Tropics) or even global scales (Logan et al., 1981). CO also leads to the formation of tropospheric ozone (O_3), an important short-lived greenhouse gas, and CO_2. CO is produced by incomplete combustion, i.e. when there is not enough oxygen to make CO_2 (van der Werf et al., 2010), such as in the case of smoldering fires. In this way, CO_2 is strongly co-emitted with CO in the presence of combustion (Bakwin et al., 1997; Potosnak et al., 1999; Turnbull et al., 2006). Previous studies used trace gases such as CO to improve the CO_2 flux estimation or to separate CO_2 emission sources. Wang et al. (2010) used the CO_2/CO correlation slope to differentiate the source signature of CO_2 and separate the different characteristics of CO_2 emissions between rural and urban sites in China. Basu et al. (2014) estimated CO_2 emissions with Greenhouse gases Observing SATellite (GOSAT) data and the Comprehensive Observation Network for TRace gases by AIrLiner (CONTRAIL) project and studied seasonal variations of CO_2 fluxes during the 2009 and 2011 period over Tropical Asia. By using the Infrared Atmospheric Sounding Interferometer (IASI) CO measurements, their study showed an increased source of CO_2 in 2010 that was caused not by rising of biomass burning emissions but by biosphere response to above-average temperatures. In addition to CO, some studies worked on the

correlation between additional species and CO_2 to constrain CO_2 emission from biomass burning. Konovalov et al. (2014) used satellite CO and aerosol optical depth data to constrain CO_2 emissions from wildfires in Siberia by estimating FRP to biomass burning rate conversion factors. Using this approach, they found that global emissions inventories underestimated CO_2 emissions from Siberia from 2007 to 2011.

As biomass burning emission estimates are necessary for constraining top-down CO_2 emissions, we want to provide our CO_2 inversion model with fire emissions that contain as much realism as possible. Fires that incorporate information from both traditional bottom-up estimation techniques and atmospheric CO data may provide a better estimate than the global inventories alone. The corresponding top-down CO_2 fluxes imposing these optimized fire emissions should have more fidelity, particularly in the Tropics, where fires and the biosphere strongly interact with one another, and especially during severe drought conditions associated with the 2015 El Niño. The objective of this paper is to assess the improvement in CO_2 biogenic emission estimates when CO-informed fire emissions are imposed, particularly during the 2015 El Niño event and the subsequent years (2017 and 2018). First, we constrain CO emissions using data from the Measurements of Pollution in The Troposphere (MOPITT). We use these optimized CO emissions together with key vegetation parameters from GFED to create an updated estimate of fire CO_2 emissions that incorporates both sets of information. Finally, these updated fire emissions are imposed in an atmospheric CO_2 inversion that constrains CO_2 fluxes, using either OCO-2 XCO_2 retrievals or in situ data, with different assumed fire emissions and appropriately rebalanced prior biogenic fluxes.

This paper is ordered as follows. The assimilation and evaluation data sets and the inversion modeling framework are described in Section 2. The results for CO and CO_2 flux estimates and evaluation against independent data are presented in Section 3. The importance of these inversion results are discussed in Section 4. Conclusions and proposed future work are presented in Section 5.

2 Data and methodology

Our experiments focus on estimation of top-down fluxes using the TM5-4DVAR system (e.g. Meirink et al. (2008); Basu et al. (2013); Crowell et al. (2018)). Our inversions are performed in sequence: (1) we assimilate total column CO retrievals from the MOPITT v8 products to produce optimized CO fluxes, which are used to update the assumed CO_2 fire emissions, and then (2) we assimilate either total column CO_2 from OCO-2 version 9 retrievals or CO_2 in situ data to produce optimized CO_2 NEE and ocean fluxes. We introduce hereafter the observations used in the inversions, the inversion system and the observations used for validation.

2.1 Data sets

2.1.1 MOPITT data

Space-based CO data are available from a large variety of instruments: IASI (Infrared Atmospheric Sounding Interferometer, Turquety et al. (2004); Clerbaux et al. (2009)) on-board Metop satellite, MOPITT (Measurements of Pollution in the

Troposphere, Drummond et al. (2010, 2016)) on-board the Terra satellite, the Tropospheric Emission Spectrometer (TES, Beer (1999)) on-board EOS-Aura and the Atmospheric InfraRed Sounder (AIRS, Aumann et al. (2003)) on-board EOS-Aqua. These satellite data can be used to monitor fire emissions from an atmospheric point of view. So far, MOPITT has been the only space-based instrument deriving CO from near-infrared (NIR), thermal infrared (TIR) and multispectral radiances (TIR + NIR). Recently, TROPOspheric Monitoring Instrument (TROPOMI, Landgraf et al. (2016)) and GOSAT-2 TANSO-FTS-2 (http://www.gosat-2.nies.go.jp/) are also retrieving CO from NIR radiances. However, MOPITT products have been consistently validated against airborne vertical profiles and ground based measurements, allowing a well-understood product (Worden et al., 2010; Deeter et al., 2019).

MOPITT (Drummond, 1993) was launched in 1999 on board the Terra satellite. Terra flies in a sun-synchronous polar orbit at an altitude of 705 km, crossing the equator at approximately 10:30 local time each morning and evening. It has a nadir view with spatial resolution of 22 x 22 km. Its swath is 650 km wide, with 116 cross-track footprints. MOPITT achieves a global coverage in about 4 days.

MOPITT uses gas filter correlation radiometry to retrieve CO mixing ratios from radiances in the 4.7 μm (TIR) and 2.3 μm (NIR) spectral bands. TIR-only retrievals of MOPITT have been shown to be mostly sensitive to CO in the mid-upper troposphere (excluding regions with strong thermal gradients such as deserts, Deeter et al. (2007)). NIR-only retrievals depend on reflected solar radiation, and are also used for retrievals of CO total column, though the vertical sensitivity is stronger near the surface than the TIR-only retrievals (Deeter et al., 2009; Worden et al., 2010). MOPITT TIR + NIR retrievals can provide improved estimates of CO near source locations and has enhanced land surface sensitivity compared to the TIR only product (Deeter et al., 2015). In this study, we consequently use the level 2 TIR-NIR profiles product in order to have better sensitivity of CO on the total column with greatest sensitivity in the lower troposphere (Deeter et al., 2013). With the observing limitations of NIR data, this product is limited to daytime observations over land. In addition, because retrievals with surface pressures less than 900 hPa might be of lower quality, they are removed for the assimilation (Fortems-Cheiney et al., 2011; Yin et al., 2015). MOPITT retrieval products are generated with an optimal estimation-based retrieval algorithm and a fast radiative transfer model involving both MOPITT calibrated radiances and a priori knowledge of CO variability (Deeter et al., 2003). The MOPITT operational fast forward model (MOPFAS) is a radiative transfer model based on HITRAN2012 (Rothman et al., 2013) database with CO parameters in log(VMR) used to simulate the MOPITT measured radiances (Edwards et al., 1999). For this retrieval method, cloud-free observations are required. The MOPITT v8 products consist of CO profile with 10 pressure levels. In our assimilation system, simulated values of log XCO using the MOPITT v8 averaging kernel are compared to the retrievals, and the difference is then propagated into flux adjustments using the TM5 adjoint.

Several studies have used inverse modelling with MOPITT data to estimate CO emissions (Huijnen et al., 2016; Yin et al., 2016; Nechita-Banda et al., 2018) and they showed that MOPITT v7 data have poor performance at detecting extreme events. However, MOPITT v8 implemented a bias correction in the radiance which demonstrated improved retrievals relative to v7 (Deeter et al., 2019). In particular, MOPITT v8 does not exhibit a latitudinal dependence in partial CO column biases observed in v7 (Deeter et al., 2019). MOPITT v8 TIR-NIR product biases are within 5% at all levels when compared to NOAA aircraft profiles. In addition, apparent long-term trends in v7 biases have been decreased to 0.1%/yr or less at all retrievals levels for

v8 products (Deeter et al., 2019). We thus expect to have better performance in the detection of extreme events by assimilating MOPITT v8 and less bias in the inferred CO emissions overall.

2.1.2 OCO-2 data

The OCO-2 (Crisp et al. (2017); Eldering et al. (2017)) satellite was launched in July 2014 as the first NASA mission dedicated to observing CO_2 from space. The satellite flies in a sun-synchronous orbit with an altitude of 705 km and a 16 day revisit time. OCO-2 passes each location at approximately 13:30 local time (Crisp and Johnson, 2005). OCO-2 observes 8 footprints across a 10 km ground track, each of which is less than 1.29 km by 2.25 km (Eldering et al., 2017). Smaller spatial footprints increase the number of cloud-free scenes allowing for more successful retrievals with lower errors (O'Dell et al., 2018), e.g. relative to the Greenhouse Gases Observing Satellite (GOSAT; Kuze et al. (2009)).

OCO-2 measures the absorption of solar reflectance spectra within CO_2 (1.6 μm and 2.0 μm) and molecular oxygen (O_2) bands (0.76 μm). Retrievals from OCO-2 have sensitivity throughout the entire troposphere with highest sensitivity close to the surface (Eldering et al., 2017). As with CO, retrievals of CO_2 from TIR observations such as those from TES or AIRS typically have lower sensitivity in the atmospheric boundary layer (Eldering et al., 2017).

CO_2 retrieval products come from the Atmospheric Carbon Observations from Space (ACOS) retrieval algorithm (O'Dell et al., 2012; Crisp et al., 2012; O'Dell et al., 2018; Kiel et al., 2019). OCO-2 radiance measurements are analyzed with remote sensing retrieval algorithms to spatially estimate column-averaged CO_2 dry air mole fraction, XCO_2. This quantity represents the average concentration of CO_2 in a column of dry air from the surface to the top of the atmosphere. ACOS XCO_2 product have been largely validated against ground-based observations from the Total Column Carbon Observing Network (TCCON; Wunch et al. (2017)). Our study uses the OCO-2 version 9 data product, as it contains all of the improvements as well as a bug fix that was found after the release of the version 8 (v8). Being a nonlinear optimal estimation product, retrievals contain residual errors that must be removed through the use of a bias correction (O'Dell et al., 2018; Kiel et al., 2019). Residual biases in XCO_2 were reduced especially over rough topography, which were found to be caused by relative pointing offsets between the three bands. Even after the bias correction is applied, errors on regional scales likely remain (O'Dell et al., 2018). Despite these shortcomings, data coverage from satellites is dense in the Tropics relative to the global in situ network, which has very few sites there. Despite the known shortcomings (biases) of satellite data, several studies have preferred to use satellite data over the Tropics to take full advantage of the improved spatial coverage. For instance, Liu et al. (2017a) and Palmer et al. (2019) have discussed the impacts of the 2015-2016 El Niño event on the carbon cycle, particularly in the Tropics using OCO-2 v7. In addition, OCO-2 retrievals have been used in several inversion models. For example, Crowell et al. (2019) showed that with different assumptions (such as a large ensemble of atmospheric inversions using different CTM, data assimilation algorithms, and prior flux), OCO-2 posterior inferred fluxes globally agree with in-situ data, but that this agreement breaks down quickly at smaller spatial and temporal scales.

To finish regarding the data we are using in our study, Huijnen et al. (2016) and Patra et al. (2017) have shown that pyrogenic CO_2 emission estimates from CO MOPITT data (through the use of emission factors) are consistent with OCO-2 measurements using a forward simulation with a CTM. With this in mind, and also that OCO-2 and MOPITT have similar vertical sensitivity

for their retrievals of CO_2 and CO, we use these two data sets to constrain surface fluxes for these two tracers. Using CO_2 and CO together in this way is an important proof of concept for upcoming missions such as GeoCarb (Moore et al., 2018), which will measure both tracers from geostationary orbit over the Americas.

2.1.3 In situ data

The in situ CO_2 data used for assimilation come from 5 collections in ObsPack format (Masarie et al., 2014). These collections include :

- the obspack_co2_1_GLOBALVIEWplus_v5.0_2019-08-12 (Cooperative Global Atmospheric Data Integration Project, 2019) which contribute to 93% of all data.

- obspack_co2_1_NRT_v5.0_2019-08-13 (NOAA Carbon Cycle Group ObsPack Team, 2019) which provides near-real time provisional observation and so the data did not get final quality control.

-obspack_co2_1_AirCore_v2.0_2018-11-13 which is provided by the balloon-borne AirCore instrument. This dataset includes almost the entire atmospheric column.

-obspack_co2_1_INPE_RESTRICTED_v2.0_2018-11-13 (NOAA Carbon Cycle Group ObsPack Team, 2018). This collection of data only comes from aircraft profiles at fives sites in Brazil.

-obspack_co2_1_NIES_Shipboard_v2.1_2019-06-12. The data come from 9 volunteer ships of opportunity operated by the Japanese National Institute for Environmental Studies (Tohjima et al., 2005; Nara et al., 2017).

These 5 collections provide around 540 assimilable observations per day. These CO_2 measurements are collected in flasks or by continuous analyzers at surface, tower, and aircraft sites (see Fig. S1) and are an important anchor for this exercise because their error characteristics are generally well-known, being directly established via calibration traceable to World Meteorological Organization standards. Additionally, these measurements provide traceability to a long history of flux estimates derived from these data as an atmospheric constraint.

2.1.4 Observations for validation : TCCON data

We evaluate our posterior model mole fractions against retrievals from TCCON, which is a ground-based network of Fourier transform spectrometers established in 2004 and designed to retrieve atmospheric gases from NIR spectra (Wunch et al., 2011). The global monthly means of the total column CO_2 measurements have accuracy and precision better than 0.25% (less than 1 ppm) relative to validation with aircraft measurements (Wunch et al., 2010, 2011). TCCON measurements have been used in several papers for validation of satellite measurements (e.g. Kulawik et al. (2016); Wunch et al. (2017); O'Dell et al. (2018); Kiel et al. (2019)). Our evaluation uses data from 23 operational instruments of TCCON globally. Table 1 lists all TCCON sites used for the evaluation and Fig. S2 shows the site locations over the globe.

Table 1. Geolocation and reference of each TCCON station used for the evaluation section.

TCCON sites	Country	Latitude	Longitude	Data revision	Reference
Eureka	Canada	80.05N	86.42W	R3	Strong et al. (2019)
Ny-Ålesund	Spitsbergen	78.9N	11.9E	R0	Notholt et al. (2014b)
Sodankylä	Finland	67.4N	26.6E	R0	Kivi et al. (2014)
Białystok	Poland	53.2N	23.0E	R2	Deutscher et al. (2019)
Bremen	Germany	53.10N	8.85E	R0	Notholt et al. (2014a)
Karlsruhe	Germany	49.1N	8.4E	R1	Hase et al. (2015)
Paris	France	48.8N	2.4E	R0	Té et al. (2014)
Orléans	France	47.9N	2.1E	R1	Warneke et al. (2019)
Garmisch	Germany	47.5N	11.1E	R2	Sussmann and Rettinger (2018)
Park Falls	Wisconsin (USA)	45.9N	90.3W	R1	Wennberg et al. (2017)
Rikubetsu	Japan	43.5N	143.8E	R2	Morino et al. (2018b)
Lamont	Oklahoma (USA)	36.6N	97.5W	R1	Wennberg et al. (2016)
Anmeyondo	Korea	36.5N	126.3E	R0	Goo et al. (2014)
Tsukuba	Japan	36.1N	140.1E	R2	Morino et al. (2018a)
Edwards	California (USA)	34.2N	118.2W	R1	Iraci et al. (2016)
Caltech	California (USA)	34.1N	118.1W	R0	Wennberg et al. (2014)
Saga	Japan	33.2N	130.3E	R0	Kawakami et al. (2014)
Izaña	Tenerife	28.3N	16.5W	R1	Blumenstock et al. (2017)
Ascension Island	UK	7.9S	14.3W	R0	Feist et al. (2014)
Darwin	Australia	12.4S	130.9E	R0	Griffith et al. (2014a)
Réunion Island	France	20.9S	55.5E	R1	De Mazière et al. (2017)
Wollongong	Australia	34.4S	150.9E	R0	Griffith et al. (2014b)
Lauder 125HR	New Zealand	45.0S	169.7E	R0	Sherlock et al. (2014)

2.2 Chemistry transport model TM5

We employ TM5 (Krol et al., 2005) and the Four-dimensional Variational (4DVAR, Meirink et al. (2008)) framework to link trace gas emissions to atmospheric tracer mixing ratios. Several inverse modelling studies have estimated CO emissions or CO_2 emissions using TM5-4DVAR (Hooghiemstra et al., 2011; Van Leeuwen et al., 2013; van der Laan-Luijkx et al., 2015; Nechitabanda et al., 2018; Basu et al., 2018; Crowell et al., 2018, 2019). TM5 is driven by 3-hourly offline meteorological fields from the ERA-Interim (Dee et al., 2011) reanalysis of the European Centre for Medium range Weather Forecasts (ECMWF). We run TM5 on a 3°x2° horizontal resolution grid for the CO inversion and on a 6°x4° horizontal resolution grid for the CO_2 inversions with 25 vertical hybrid sigma-pressure levels. The initial condition for CO is globally constant to 80ppb, which is then combined with a 6 month spin-up to account for discrepancies from the real atmospheric distribution of CO. The initial global distribution of CO_2 is taken from the CarbonTracker (Peters et al. (2007) version CT2017, with updates documented

at http://carbontracker.noaa.gov) posterior mole fractions. The CT2017 fields are constrained over the period 2000-2016 with data from the global in situ network. Both inversions are run from July 1, 2014 until March 1, 2019, i.e. with six months of spinup and two months of spindown to avoid so-called "edge effects" affecting the period of interest from 2015-2018.

The CO sink from OH is represented in TM5 by a monthly OH climatology from Spivakovsky et al. (2000). This OH climatology is scaled by a factor 0.92 based on methyl chloroform simulations (Huijnen et al., 2010).

2.3 Inversion system and analyses

We use TM5-4DVAR to infer fluxes as the long window ensures a long term spatio-temporal distribution of the trace gas in the atmosphere that is consistent with multi-year flux distributions. The TM5-4DVAR model is used in this study to estimate CO and CO_2 emissions with the corresponding satellite and in situ. TM5-4DVAR utilizes optimal estimation to minimize a Bayesian cost function (Rodgers, 2000) in order to find the state vector corresponding to surface emissions of CO or CO_2 that best match the observations within their relative uncertainties. The a posteriori flux is found by minimizing the mismatch between the forward model and the observations weighted by the inverse of the observation error covariance matrix **R** while staying close to a set of a prior fluxes weighted by the inverse of the a priori error covariance matrix **B**. These matrices are discussed in more detail in Section 2.3.1. Although the CTM is quasi-linear, the observation operator for CO is not. Since we use log(VMR) for the MOPITT retrievals as the CO observable, the non-linear optimizer M1QN3 from Gilbert and Lemaréchal (1989) is employed. Both the transport and observation operators for CO_2 are linear, and so we employ the conjugate gradient method to estimate the optimal CO_2 emissions, the implementation of which is described in great detail in Basu et al. (2013).

2.3.1 A priori information

a) CO parameterizations

Injection heights, in the CO inversion, are computed using IS4FIRES (Integrated System for Wild-Land Fires, http://is4fires.fmi.fi/, Sofiev et al. (2013)). This emission database is driven by re-analysis FRP obtained from MODIS (Giglio et al., 2006)) instrument on board Aqua and Terra satellites.

Three emissions categories are used for the CO inversion : anthropogenic (which represents the combustion of fossil fuels and biofuels), natural sources (direct CO emissions from vegetation and oceans) and biomass burning (vegetation fires). In our configuration, we only optimize biomass burning emissions.

Anthropogenic emissions come from MACCity inventory (Granier et al., 2011). This inventory provides projected inter-annual trends in the anthropogenic CO emissions.

The oxidation of CH_4 and non-methane volatile organic compounds (NMVOCs) such as isoprene (C_5H_8) and monoterpene ($C_{10}H_{16}$) leads through photolysis and reaction with OH to the formation of formaldehyde, the major chemical source of CO (Atkinson, 2000). Isoprene is a member of the group of hydrocarbons known as terpenes. It is explicitly taken into account in TM5 as it represents the dominant biogenic NMVOC emission (Guenther et al., 2012). Isoprene and monoterpene oxidation schemes are based on the mechanisms developed by Yarwood et al. (2005). Isoprene contributes to 9-16 % of the global CO

burden (Pfister et al., 2008). They account for 68% in TM5 of the biogenic NMVOC emissions that react to produce CO. By contrast, monoterpene accounts for 15% (Tsigaridis et al., 2014). The chemical production of CO coming from the oxidation of methane and NMVOCs requires monthly 3-D CO fields produced by oxidation of biogenic and anthropogenic hydrocarbons including CH_4. We use chemical production of CO from the oxidation of CH_4 and from NMVOCs by using a 2010 simulation with the full chemistry version of TM5 (Huijnen et al., 2010).

A priori biomass burning CO emissions are taken from GFED4.1s inventory (van der Werf et al., 2010) and incorporate a daily cycle. GFED4.1s burned area are based on fire observations from the MODIS instrument with a 500 m horizontal resolution (further description in GFED versions can be found in Appendix A). The MODIS burned area data have been combined with active fire data from Tropical Rainfall Measuring Mission (TRMM), the Visible and Infrared Scanner (VIS), and the Along-Track Scanning Radiometer (ATSR), three other instruments on board with MODIS. GFED4.1s has a spatial resolution of 0.25°x0.25° and includes estimates of burned area, carbon emissions, monthly biospheric carbon fluxes based on the CASA-GFED4s framework and the information from small fire fraction. Additionally, monthly carbon emissions of GFED4.1s distinguish between different vegetation types such as boreal forest, agricultural waste, temperate forest, deforestation, peatland, and savanna.

The prior uncertainty covariance matrix **B** is described by a product of uncertainty variance and correlations in space and time. Spatially, a Gaussian correlation length scale of 1000 km is used, as justified in Meirink et al. (2008), while we assume the prior errors have a temporal correlation scale of 4 days. As in Hooghiemstra et al. (2011, 2012) and Nechita-Banda et al. (2018), an uncertainty standard deviation of 250% has been applied for the grid-scale prior of biomass burning emission. This large uncertainty is assumed since these inventories support large uncertainties. As mentioned by Hooghiemstra et al. (2011), this yields between 40-100% of prior continental emissions uncertainty, depending on the region. The errors are assumed uncorrelated leading to a diagonal observational error covariance matrix **R**.

b) Computation of an optimized CO_2 Fire Prior

In this section, we describe the computation of our optimized prior fire emission (FIREMo) which we will use to observe the impact of CO fire emissions in posterior CO_2 biospheric fluxes. The steps of FIREMo calculation are shown in Fig. 1. For each pixel of CO posterior fire emissions, we applied a vegetation fraction based on the dry matter product (DM) of GFED4.1s. We obtained fire emissions for each monthly vegetation type (savanna, boreal forests, peat, temperate forests, deforestation and agriculture waste). Figure S3 shows GFED DM vegetation type for each year over land, where each pixel represents one or more vegetation types.

We first calculated the emission ratios $ER_{(CO/CO_2)}$ which allowed us to convert CO fire emissions to CO_2 fire emissions. The emission ratios are computed using GFED emission factor for each vegetation type (annotated *i* in the equation 1). Following the equation of Andreae and Merlet (2001) :

$$ER_{(CO/CO_2)_i} = \frac{EF_{CO\,i}}{EF_{CO_2\,i}} \cdot \frac{M_{CO_2}}{M_{CO}} \tag{1}$$

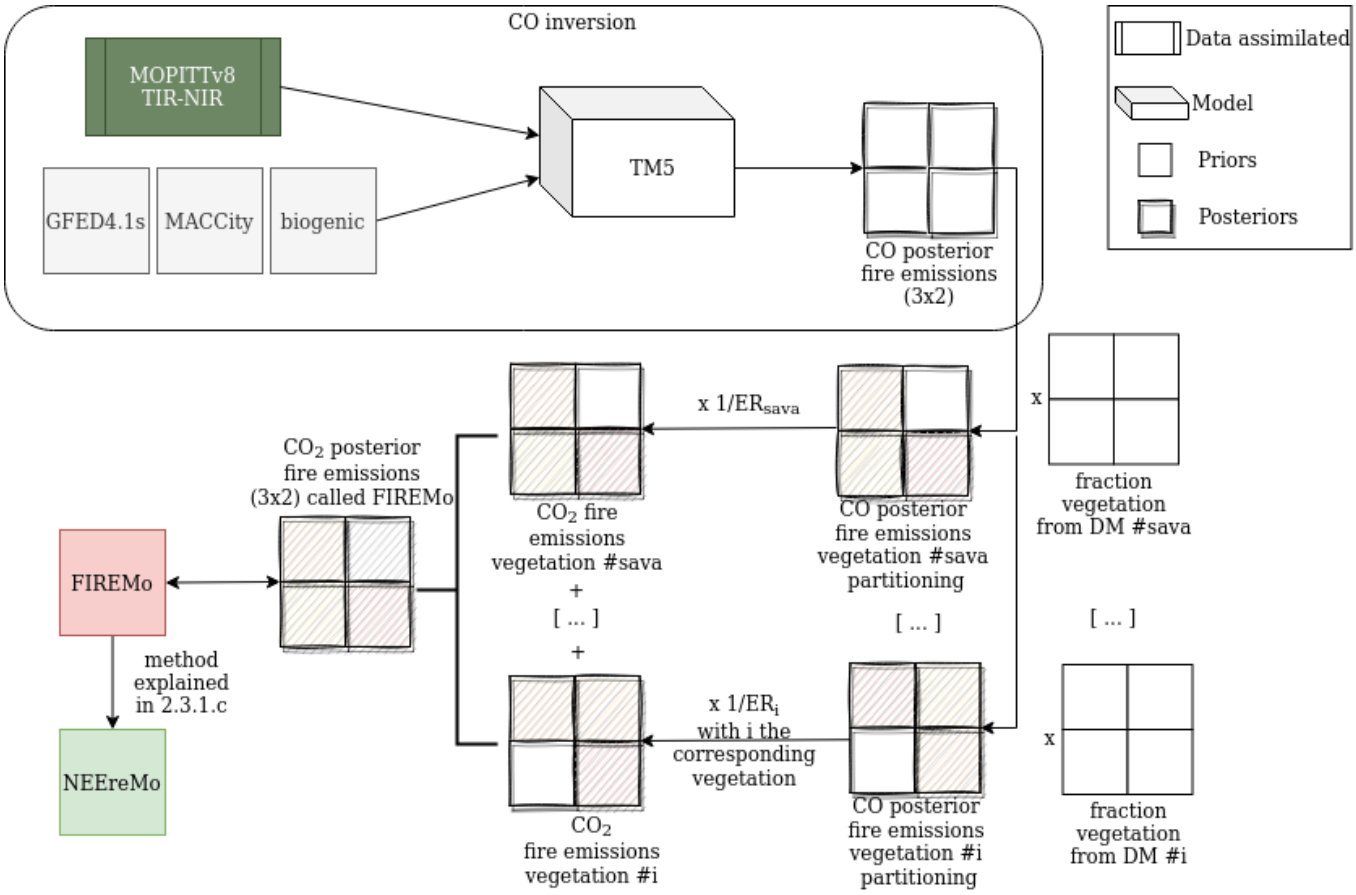

Figure 1. Flowchart of the FIREMO calculation

with $M_{CO} = 28$ g.mol^{-1} and $M_{CO_2} = 44$ g.mol^{-1} the molecular weights of CO and CO_2; EF are the emission factors for each vegetation types describes in table 2. Emission factors allow us to estimate trace gases emissions from carbon losses during fires (Andreae and Merlet, 2001). For better comparison and as the CMS-GFED3 product (we will introduce later) used the emission factor of Andreae and Merlet (2001) and Akagi et al. (2011), we applied the same emission factors and consequently did not use the new estimate established by Andreae (2019).

Table 2. Emission Factors in $g.kg^{-1}.DM^{-1}$ for CO and CO_2, and emission ratios $ER_{(CO/CO_2)}$ available from GFED4.1s by vegetation types based on van der Werf et al. (2017).

	Savanna	Boreal forests	Temperate forests	Deforestation	Peat	Agriculture waste
EF_{CO}	63	127	88	93	210	102
EF_{CO_2}	1686	1489	1647	1643	1703	1585
$ER_{(CO/CO_2)}$	0.059	0.134	0.084	0.089	0.194	0.101

We then aggregated the 0.25°x0.25° vegetation fraction partitioning of GFED to create vegetation fraction product at a 3°x2° grid (see Fig. 1). We applied this aggregated fraction to the posterior simulated CO fires, which partitioned the posterior CO fires by vegetation types. Finally, the emission ratio for each vegetation type was divided into the posterior CO fire partitioned for each vegetation type (Basu et al., 2014). This results in monthly CO_2 emission per vegetation type at a 3x2 resolution. Finally, we sum up these emissions across all surface types in order to get monthly total optimized prior CO_2 biomass burning emissions that we called "FIREMo" (see Fig. 1). We used this FIREMo as a fire prior emissions in CO_2 inversions along with a re-balanced respiration and NEE (in balance with fire estimate), using the parameterization described in the following section 2.3.1.c.

c) CO_2 parameterizations

CO_2 emissions are separated into four categories: anthropogenic sources, ocean fluxes, terrestrial biosphere fluxes (meaning the sum of the photosynthesis and respiration) and fires.

The anthropogenic emissions are taken from the Open-source Data Inventory for Anthropogenic CO_2 2018 (ODIAC2018; Oda and Maksyutov (2011)). A diurnal cycle is imposed by TIMES product with weekly scaling as suggested by Nassar et al. (2013). Fossil fuel emissions are not optimized in the CO_2 inversions, as is typical of global tracer transport inversions (e.g. Peylin et al. (2013); Crowell et al. (2019)). Ocean fluxes are taken from Takahashi et al. (2009). They are assumed to have an uncertainty variance of 50%. Both biospheric and oceanic emissions are optimized in the CO_2 inversions. The uncertainties in the prior fluxes are derived from different climatological fluxes with exponential spatio-temporal correlation assumed. For the oceanic component, the horizontal correlation is 1000 km and the timescales is 3 weeks, while for the terrestrial component, length and timescale are 250km and 1 week. These uncertainties are applied similarly to all experiments.

Terrestrial biosphere fluxes and fire emissions are difficult to disentangle from CO_2 data alone, and some inverse modeling studies (e.g. Crowell et al. (2019)) choose instead to report the net land fluxes. Likewise, some global land flux estimates such as GEOS-Carb CASA-GFED3 project (Ott, 2020) use fire estimates to revise the terrestrial biosphere flux estimates through modification of ecosystem respiration. We take a similar approach, starting with the gross primary production and respiration estimates from the CASA-GFED3 3-hourly $0.5° \times 0.625°$ (Ott, 2020). We then modify the net flux in concert with each fire emissions estimated as follows.

Net ecosystem exchange (NEE) in the CASA-GFED3 product is expressed as the sum of heterotrophic respiration (Rh) and gross ecosystem exchange (GEE) :

$$NEE3 = Rh3 + GEE3 \tag{2}$$

We modified the respiration from CASA-GFED3 (*Rh3*, respiration linked to FIRE3) to create respiration estimates for GFED4.1s (*Rh4*, respiration linked to FIRE4) and FIREMo (*RhMo*, respiration linked to FIREMo) which balance with the updated CO_2 fire estimate so that estimated respiration increases (decreases) in the places where each fire estimate is smaller (larger) than

FIRE3 (GFED3):

$$Rhx = Rh3 + max(FIRE3 - FIREx, 0) \tag{3}$$

where x is either “4" or “Mo". This equation means that the difference between FIRE3 and FIREx is cut off at 0 when the difference is negative. With this equation we only consider the positive difference (when we have lower FIREx emissions than FIRE3). The resulting net ecosystem exchange, i.e. NEE4 or NEEMo, is then computed using (2), with *GEE3* used for both NEE4 or NEEMo equations. We then apply a simple rebalancing scheme to match the yearly NOAA global mean growth rate (AGR_{NOAA}) for 2015-2018 (see table 3), since

$$\text{AGR} = \overline{\text{NEE}} + \overline{\text{FIRE}} + \overline{\text{FOSSIL}} + \overline{\text{BIOFUEL}} + \overline{\text{OCEAN}} \tag{4}$$

where $\overline{X}$ represents the global total annual flux for category X. We use ODIACv2018 (with 2018 repeated for 2019) to compute the global fossil fuel totals (values in the table 3), BIOFUEL from the CASA land biosphere model (van der Werf et al., 2004), and a fixed annual value of -2.6 PgC/yr for the oceans for simplicity, and we use FIRE from each source described above.

Table 3. Global total fossil fuel emissions, fire from GFED3 and GFED4.1s, FIRE (fire+biofuel), biofuel emissions and AGR from NOAA in PgC/yr.

	2015	2016	2017	2018
BIOFUEL	0.479	0.476	0.486	0.486
FOSSIL FUEL	9.89	9.91	10.07	10.28
GFED3	2.03	1.63	1.97	1.97
GFED4	2.09	1.73	1.78	1.69
FIRE3	2.51	2.11	2.46	2.46
FIRE4	2.57	2.21	2.27	2.18
FIREMo	1.82	1.47	1.58	1.56
NEECMS	-3.23	-3.09	-5.11	-4.82
NEEre3	-3.22	-3.08	-5.11	-4.82
NEEre4	-3.23	-3.15	-4.83	-4.49
NEEreMo	-2.50	-2.43	-4.24	-3.93
AGR_{NOAA}	4.3	6.3	6.06	4.54

Any mismatch between the AGR derived from our prior flux estimates (AGR_x) and AGR_{NOAA} is assumed to be due to an incorrect estimate of global NEE. We adjust NEE at each gridpoint with a simple scaling on global total respiration (i.e. Rhx) and GEE:

$$\text{AGR}_{\text{NOAA}} - \text{AGR}_x = (1+k)\overline{\text{Rhx}} + (1-k)\overline{\text{GEE}}. \tag{5}$$

where x is either 3, 4, or Mo, depending on whether we use FIRE3 (GFED3), FIRE4 (GFED4.1s), or FIREMo. This equation is easily solved for k using each annual global total, and the resulting corrections are applied to each 3-hourly gridded value

of GEE and respiration for each choice of fire emissions. In this way, the a priori global CO_2 emissions are ensured to match the annual global growth rate as measured by NOAA regardless of the fire emissions assumed, as well as a spatial pattern and seasonality that aligns with bottom up models' GEE and Rh estimates as closely as possible.

Table 4. Experimental Configurations

	CMS-GFED3	GFED3re	GFED4re	MOre
ODIAC Fossil	X	X	X	X
FIRE3 (GFED3 Fires)	X	X		
FIRE4 (GFED4.1s Fires)			X	
FIREMo (MOPITT Fires)				X
Takahashi Ocean Flux	X	X	X	X
Annual Total Matches AGR_{NOAA}		X	X	X

We run the CO_2 inversions with the re-balanced terrestrial biosphere net flux NEEre*x* corresponding to either FIRE3, FIRE4 or FIREMo priors. In order to assess the impacts of the rebalancing procedure, we perform a fourth experiment that assumes the GEOS-Carb CASA-GFED3 NEE as the prior biosphere flux with GFED3 fires, and the results are labeled in what follows as CMS-GFED3. All CO_2 FIRE priors include both biomass and biofuel burning. The details of each of the 4 priors and the experimental configurations are detailed in table 4.

In this study, several inversions were performed with the TM5-4DVAR inversion framework. MOPITT v8 L2 CO data were assimilated to constrain fire emissions of CO. Separately, OCO-2 v9 XCO_2 and in situ CO_2 are used to constrain net fluxes of CO_2 (see Fig 2).

We optimized CO biomass burning emissions and CO_2 biospheric and oceanic emissions on a weekly basis.

3 Results

In section 3.1, we examine the impacts of assimilating MOPITT v8 XCO observations on inferred fire CO emissions after vegetation partition and the comparison with the prior GFED4.1s CO emissions categorized by vegetation type.

In section 3.2, we focus on the CO_2 inversions. As fire emissions are not optimized in CO_2 inversions, we will examine how posterior NEE varies according to observation constraint and the imposed fire fluxes. We first compare (in 3.2.1) the variability and magnitude between the fire and biospheric priors used in the CO_2 inversions over the globe and zonal bands. Coparison are also done over the same regions as in Crowell et al. (2019), which are Transcom (Gurney et al., 2002) regions that are further subdivided at the equator (which we will called OCO-2 MIP regions). The regions are defined in Fig. 3 and are composed of 16 land regions and 11 ocean regions. We will focus on regions over land, as we are mostly interested in the interplay between assumed fire emissions and inferred NEE. We then investigate the covariation of imposed CO_2 fire emissions and optimized NEE with OCO-2 data and in-situ data (3.2.2). Finally, posterior simulated CO_2 mixing ratio are validated against TCCON data over the globe in section 3.2.3.

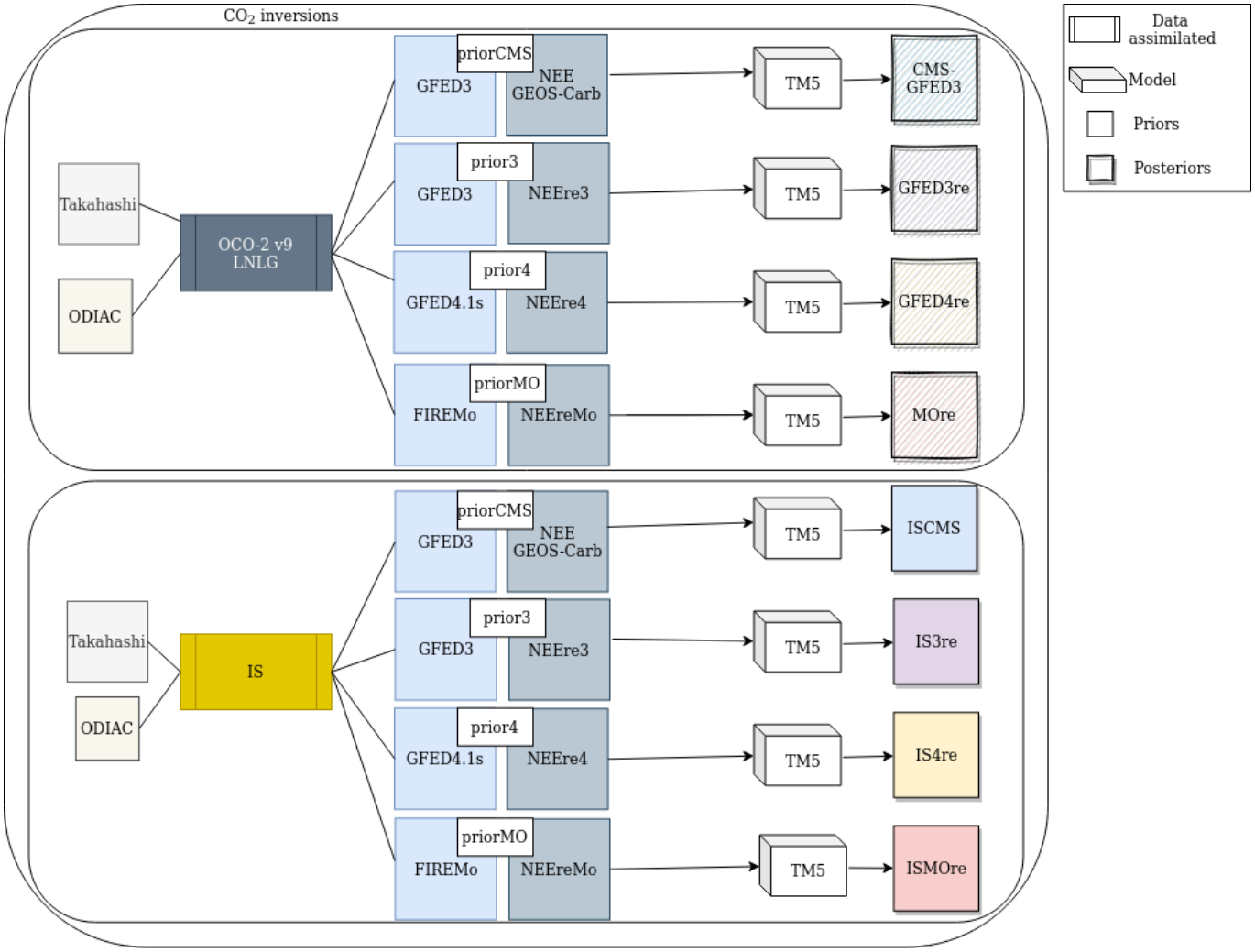

Figure 2. Flowchart of the six different CO_2 inversions performed.

3.1 Fire CO emissions partitioned by vegetation type : MOPITT optimized emissions versus GFED4.1s emissions

Figure 4 shows the annual CO posterior and prior fire emissions split by vegetation combustion across the globe and by OCO-2 MIP regions. Overall, it can be seen that depending on the region, the assimilation of MOPITT data involves less or more CO emissions compared to the prior GFED4.1s.

For North Temperate America, posterior emissions remain close to the prior estimates, suggesting that the inferred emissions are consistent with GFED4.1s. Comparable results are also observed for Temperate North Africa. However, this region is known to have a lot of Saharan dust transported across the Atlantic Ocean and towards Europe most of the year, which could explain the posterior emissions being close to the prior as those MOPITT soundings have largely been removed by pre-screeners.

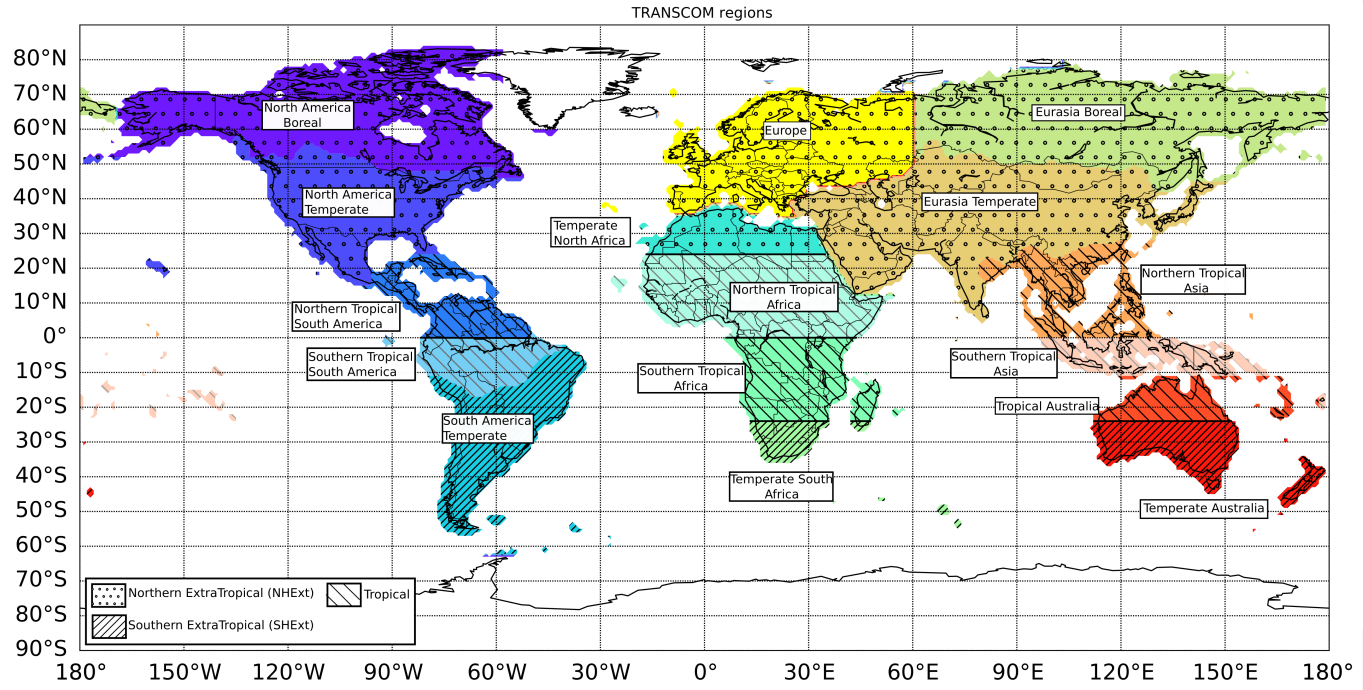

Figure 3. OCO-2 MIP regions for which prior and posteriors gridded fluxes are aggregated for comparison

North Tropical Africa is not only affected by dust, but it is also largely affected by clouds during the wet season of the African monsoon (from May to August), which could lead to errors in retrievals that pass the pre-screeners. The combination of clouds and dust could explain the MOPITT posterior fires having lower emissions than the prior GFED4.1s estimate. But further investigation into North Tropical Africa is needed. Even though the prior is higher than the posterior for tropical Africa, in opposition to the previous multi-species study of Zheng et al. (2018a), the posterior emissions better fit MOPITT measurement than the prior (Fig. S4). Tropical south America (including North Tropical South America and South Tropical South America) is also known to have cloud coverage limiting satellite observations. We however observe similar emissions between the prior and the posterior for the northern region, with slightly higher emissions for MOPITT. For the southern region, differences between the prior and the posterior are strong. The cloud coverage might explain this behavior, but further investigation are needed for these two regions.

The discrepancies observed for Eurasia temperate between MOPITT and GFED4.1s could be that the vegetation type is not well represented for these regions. As mentioned in Pechony et al. (2013), agriculture and savanna vegetation types might not be the dominant burning vegetation type over North Africa and the Middle East, since these regions have seen an increase in croplands area well control by human activities and so burn rarely. However, Kazakhstan is a region of temperate forest often dominated by fires (Venevsky et al., 2019), a characteristic that MOPITT posterior emissions seem to observe as mush as the prior GFED4.1s.

Figure 4. Annual CO fire emissions by vegetation type over the OCO-2 MIP regions between fire priors (hatch bars) and fire posterior from 2015 through 2018. Vegetation types are representing by colors : agriculture in gray, deforestation in yellow, savanna in dark-red, temperate forest in blue, peat land in red and boreal forests in green. Emissions are annually in TgCO/yr.

We can also observe that over Northern Tropical Asia, MOPITT fire emissions are higher than GFED4.1s (see Fig. 4 and Fig. S7). This is observed for all years, where MOPITT emissions are almost 5 TgCO/yr (2 TgCO/yr) for savanna (for the

other vegetation types) higher than from GFED4.1s. As mentioned in Pétron et al. (2002) and Arellano et al. (2004), CO emissions in Northern Tropical Asia are significantly underestimated in current inventories. Previous studies have shown that peat area and depth, producing large amount of carbon (0.60 PgC/yr which represents 26% of the total carbon fire emissions, Nechita-Banda et al. (2018)), were found to have significant uncertainties in Indonesia in the emissions inventories (Lohberger et al., 2017; Hooijer and Vernimmen, 2013). Our posterior have lower emissions than the prior for southern tropical Asia, in contradiction to what Nechita-banda et al. (2018) observed. However, Nechita-banda et al. (2018) assimilated MOPITT and NOAA observations and used GFAS as fire priors, an inversions set-up different to what we used. Additionally, no evaluation against independent data have been performed in their study to determine if their results are more trustworthy than our results.

Moreover, our posterior can capture the seasonality of peat fires over Indonesia in comparison to GFED4.1s. Figure S6 shows for Southern Tropical Asia (mainly visible in 2015 due to the large emissions) that GFED4.1s have a fire peak earlier than MOPITT. van der Laan-Luijkx et al. (2015) and Nechita-banda et al. (2018) hypothesized that GFED4.1s might not capture the timing of emissions over area with peat fires due to the use of burned area, which may be more sensitive to the initial stages of the fire than to the continued burning.

3.2 OCO-2 and in situ CO_2 inversions with different fire and NEE priors

We performed inversions with different CO_2 fire and NEE priors assimilating: i) OCO-2 XCO_2 retrievals and ii) CO_2 in-situ data. See Fig. 2 for details of the eight CO_2 inversions.

To investigate the uncertainty in inferred CO_2 emissions arising from the selection of fires, we perform CO_2 inversions with three different global gridded fire estimates. The first one is taken from the GEOS-Carb CASA-GFED3 product (Ott, 2020), which we label “FIRE3"; for the second we use GFED4.1s, denoted “FIRE4". The third set, denoted “FIREMo", is described in Section 2.3.1.b. The methodological differences between FIRE3 and FIRE4 are described in the appendix A.

3.2.1 Prior NEE and fires CO_2 fluxes

Figure 5 shows annual CO_2 emissions for the prior estimates in global and by latitude bands from 2015 through 2018. The prior categories shown are fire, NEE and net fluxes for the prior4 (FIRE4, NEE4re), prior3 (FIRE3, NEE3re), priorMO (FIREMo, NEEMore) and priorCMS (FIRE3, GEOS-Carb). At the global scale, the three non-CMS priors (prior3, prior4, and priorMo) give the same net sink of carbon for the whole period (matching the NOAA AGR with the same assumed fossil and ocean fluxes), decreasing from 2015 through 2018. The priorCMS gives net sources of carbon increasing in time. Global fire emissions as well as net carbon fluxes, of the non-CMS priors, are within the spread of estimation of the Global Carbon Budget estimated by Le Quéré et al. (2018) and Bastos et al. (2018). The decrease (increase) in NEE sinks (net sources) for priorCMS during the period of study is driven by the fact that the product imposes a long term balance between fire and NEE and is not constrained to match the measured growth rate of CO_2 in the atmosphere. The discrepancy shows up particularly in the Northern Hemisphere Extra-Tropics (NH Ext) and Southern Hemisphere Extra-Tropics (SH Ext) where sinks of priorCMS are generally smaller than the others.

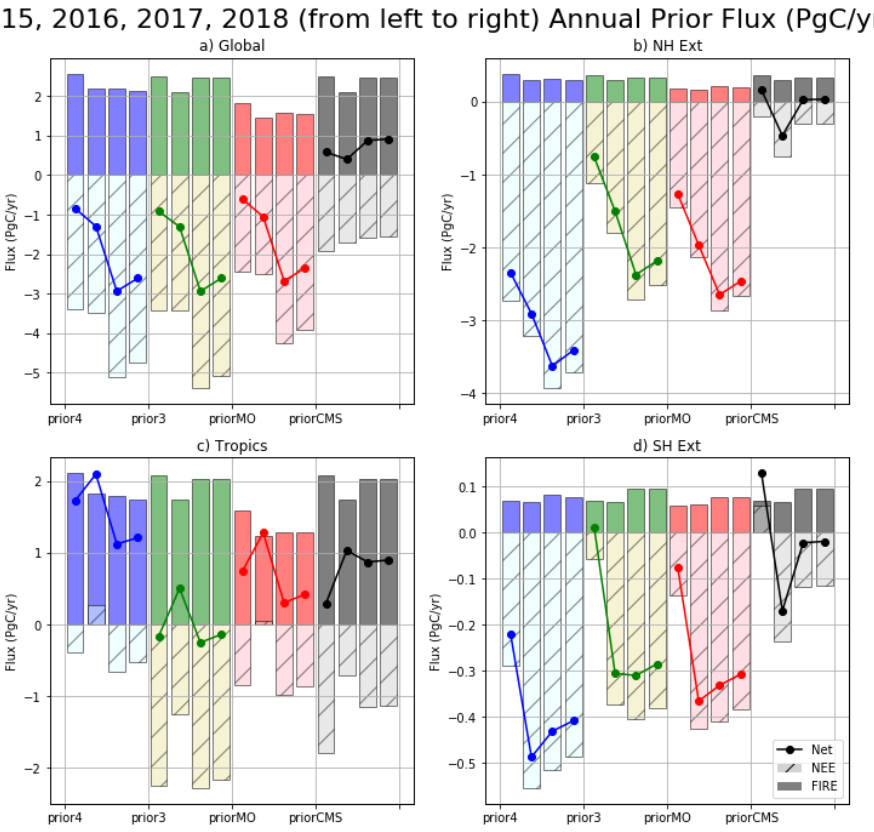

Figure 5. Annual prior CO_2 emissions, in global and by latitude bands, used later in top-down inversions. Annual net flux (lines), NEE (bars with hatches) and FIRE (bars with darker colors) prior emissions are represented from 2015 through 2018 (left to right) between GFED4.1s (blue), GFED3 (green), MOPITTopt (red) and CMS (black).

We can observe that FIRE4 and FIREMo priors have a deeper Northern Hemisphere sinks than FIRE3 (particularly observed for Europe and Northern Asia, Fig. 5 and Fig. 6), which is balanced by stronger net sources over the Tropics (coming mainly from Southern Tropical Africa and Southern Tropical Asia respectively, Fig. 6). The scaling of GFED3 GPP and respiration to match the global AGR yields deeper biogenic sinks over the Tropics than with all the other priors. We can also observe for Southern Tropical Africa that FIRE4 has larger fires than FIREMo, consistent with the fact that GFFED4.1s CO was observing higher CO fire emissions than MOPITT (Fig. 4 and Fig. S7).

The global fire emissions indicate that FIREMo yields less emissions compared to all other priors, a difference coming from tropical regions. These lower fire emissions observed by FIREMo in the Tropics come mainly from Tropical Australia (with values in 2015 of ∼0.05 PgC/yr), Tropical Africa (∼0.35 PgC/yr) and Southern Tropical South America (∼0.1 PgC/yr). But larger fire emissions are observed with FIREMo in Southern and northern Tropical Asia compared to FIRE4. The larger

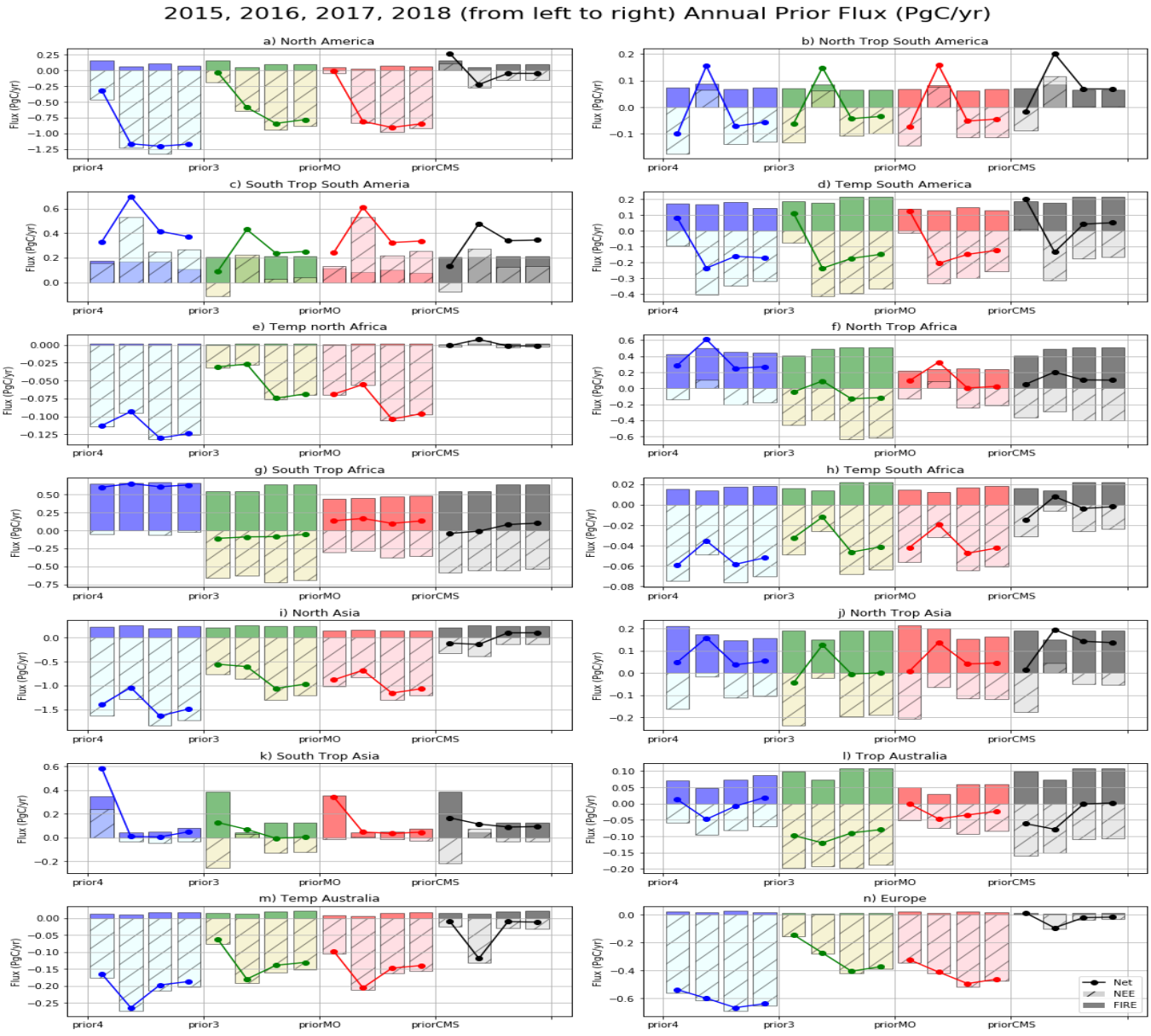

Figure 6. Same as Fig. 5 but for all OCO-2 MIP regions (from left to right, top to bottom) : north America, North Tropical South America, South Tropical South America, Temperate South America, Temperate North Africa, North Tropical Africa, South Tropical Africa, Temperate South Africa, north Asia, North Tropical Asia, South Tropical Asia, Tropical Australia, Temperate Australia, and Europe.

emissions with FIREMo compared to FIRE4 over tropical Asia comes mainly from savanna (the main vegetation type in this region, see Fig. S8).

As already observed with the CO emissions (Fig. S6) and discussed in van der Laan-Luijkx et al. (2015) and Nechita-banda et al. (2018), the seasonality of fires over tropical Asia is better captured with MOPITT than with the emission inventories for peat lands. However, this is not only true for peat but also for other vegetation types. For savanna, agriculture and peat lands, FIREMo observed a peak in fire seasonality after the peaks observed with GFED (Fig. S9). This is particularly true for the 2015 El Niño fires but less for the fires that occurred in 2017 and 2018. In this period, FIREMo does not observed as much fire emissions as GFED with a similar seasonality. The difference in seasonality for 2015 could be a result of the large and intense fires during the El Niño event burning larger regions and releasing more smoke which could have impacted the MODIS burned area data used in GFED but probably also the MOPITT retrievals. Further investigation are then needed to study this region.

3.2.2 Comparison between the CO_2 posterior fire and biospheric emissions : impact of re-balanced NEE and fire prior in CO_2 posterior emissions

We assimilated OCO-2 and in situ data separately in order to assess the impact of these data in conjunction with different fire emissions and corresponding land flux priors. In all inversions, only NEE and ocean fluxes have been optimized.

a) Global and latitudinal flux

Figure 7 shows global and latitudinal annual net fluxes, FIRE and NEE fluxes for both OCO-2 and in situ (IS) inversions. We can see that globally, net fluxes for OCO-2 posterior emissions across the different priors are consistent. The sinks seem to adjust the different fire contributions. This is also observed for the IS inversions.

The range of net flux observed with all OCO-2 inversions are consistent with other studies (Palmer et al., 2019; Crowell et al., 2019; Peiro et al., 2022). Global sinks are larger with IS inversions than with OCO-2 ones. These sinks observed with IS are driven by larger sinks in the tropics (Fig. 7). CMS-GFED3 and ISCMS posterior emissions seem to have slightly weaker sinks than the other posteriors. The imposed AGR seems then to have an impact at latitudinal scales.

The Northern Hemisphere Extra-Tropics (NH Ext) posterior fluxes are consistent across the different priors for both observation constraints, which is not surprising given the good coverage of the in situ observations in this region. The consistency across the priors for the Northern latitude bands are also observed in the simulation study of Philip et al. (2019) where they used different NEE priors to observe the impact on the OCO-2 posteriors. For OCO-2 inversions, we can see small variations from year to year (going to -2.5 PgC/yr in 2015 through -2.75 PgC/yr in 2016) except for 2018 where the net sink drops to -2 PgC/yr.

SH Ext shows similar fluxes across the priors for each data constraint. However, 2016 is adjusted downward significantly for the OCO-2 fluxes (between -0.4 PgC/yr and -0.6 PgC/yr) compared to the in situ fluxes (between -0.2 PgC/yr and 0.1 PgC/yr), balanced with stronger sources over the Tropics. This result suggest a transport connection between the Tropics and SH Ext fluxes with the OCO-2 inversions, where land coverage is limited and hence retrievals are sparser than the other regions. On

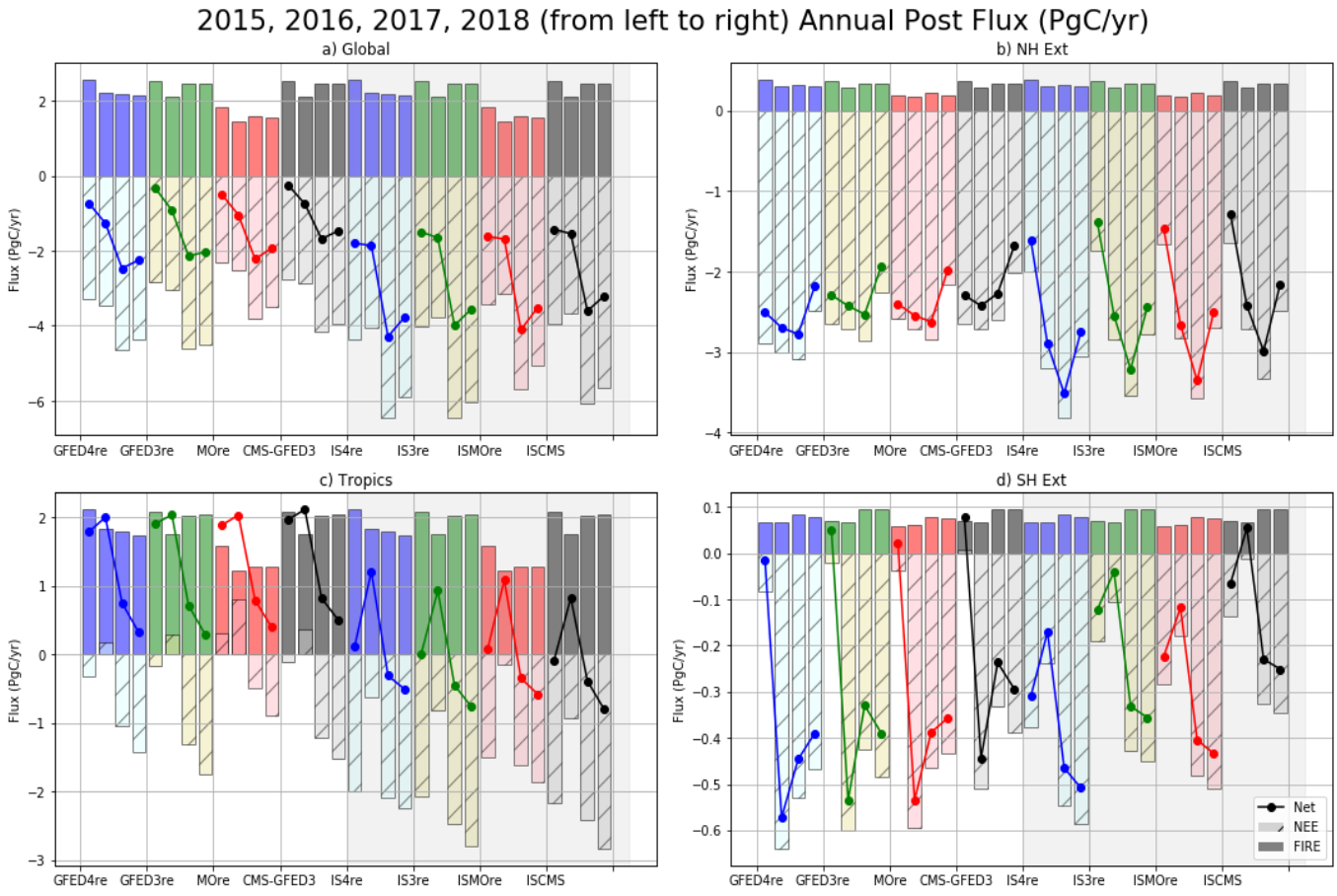

Figure 7. Global and latitudinal CO_2 posterior emissions between OCO-2 and in situ inversions as GFED4re (in blue), GFED3re (in green), CMS (in black) and MOre (in red). Annual fluxes are displayed from 2015 (left) through 2018 (right). FIRE emissions are darker colored bars, NEE fluxes are hatched bars and lines depict the net land fluxes.

the other hand, this does not seem to be the case in the in situ results, but we know that there are a few in situ data present in the SH Ext and so they have a different data constraint.

For the Tropics, we can again observe a consistency in OCO-2 across the priors. The intense fires and CO_2 sources related to the 2015 El Niño Oscillation over the Tropics and mainly Indonesia might not be seen with in situ data due to their weak coverage in these regions. This could then explain the larger sinks with in situ NEE emissions. Even though we observe a consistency across the priors, MOre and ISMOre have a smaller sink in 2015 (with sources for OCO-2 inversion) compared to the other inversions in order to balance the 0.5 PgC/yr smaller fires that FIREMo gives. This balance was also observed for the priors (see Fig. 6). The net fluxes of ISMOre and IS4re look similar for the Tropical regions, while the net fluxes of IS3re and ISCMS look alike, suggesting the sensitivity in these regions to the fire prior, not only for IS but also for OCO-2 data constraint.

b) Regional fluxes

When we compare the posterior regional fluxes, we can see difference in the carbon balance.

If we first look the Northern Extra-Tropical regions (North America, North Asia and Europe), we can see that the OCO-2 inversions have deeper net sinks than IS (see Fig. 8). The in situ data are placing almost all of the NH Ext sink over Northern Asia, but are placing sources of carbon over North America for 2015. In-situ data do not have an homogenize coverage over the NH Ext band: large number of observations are situated over Temperate North America and Europe but are very sparse over the Boreal regions and Temperate Eurasia (see Fig. S1). The large differences in net sinks occur then over the regions with few data (north Asia regions).

It is interesting also to see balance between the regions in Northern Hemisphere with Southern Hemisphere. For instance, it seems that the sink decreased for 2018 (starting in 2017) observed with both IS and OCO-2 over North Asia is balanced by net sinks in tropical Asia (North and South). The deeper sinks observed with OCO-2 in Europe are also anti-correlated with the net sources observed in Northern Tropical Africa (Fig. 7). Reuter et al. (2014) found a similar mass balance, using GOSAT data, uptake of around 1 PgC/yr which was 0.5 PgC/yr higher than expected from in situ inversions. However, as mentioned in Reuter et al. (2017), there is a lack of carbon budget information over Europe and there is hence no reliable benchmark for comparison. The balance observed here between IS and OCO-2 inversions was also observed in the study of Peiro et al. (2022). However, for Europe, we can see that the variability in our priors is different than the ones used in Peiro et al. (2022). A major difference between this study and Peiro et al. (2022) is that the rebalanced priors and posterior fluxes provide the largest sink in 2017, as opposed to 2016. This is likely a consequence of the larger fires and the subsequent rebalanced respiration that was derived in our study.

Across the different fire emissions we observe a split: MOre and GFED4re inversions (respectively ISMOre and IS4re) are similar, while GFED3re and CMS-GFED3 (respectively IS3re and ISCMS) are more similar. That means fires have a larger impact on the posterior solution than the rebalancing of prior NEE to match the global AGR. We can observe that for almost all regions, the sinks with NEE4re and NEEMore are deeper than with NEE3re and Geos-Carb CMS but are balanced with larger sources in other regions, mainly over the Tropics (Fig. 7).

Focusing on the Tropical regions, OCO-2 fluxes are consistent for each priors. For Northern Tropical South America (Fig. 8), OCO-2 fluxes have around 0.5 PgC/yr efflux during the El Niño period (2015-2016) and neutral emissions during the 2017-2018 period. IS fluxes are also strong during the El Niño period, but remain moderately high in 2017. As observed in the Fig. 1 of the paper of Peiro et al. (2022), which used the same set of IS data, the number of IS data does not decrease significantly, meaning that changing observational coverage is not the cause of this behavior. The number of in situ observation is particularly low in the tropics compared to the extra-tropical southern and northern hemispheres (Fig. 2 of Peiro et al. (2022)). One possible explanation is the lag between flux in the Tropics and observation coverage by the in situ network, which could be aliasing flux signals in time, though this hypothesis is difficult to test. Very large differences between the IS and OCO-2 inversions appears for Southern Tropical South America (Fig. 8). The OCO-2 posteriors emissions seem to be closer to the priors than the IS are. One explanation for that has been mentioned previously in Peiro et al. (2022). The cloud coverage above the moist Amazon

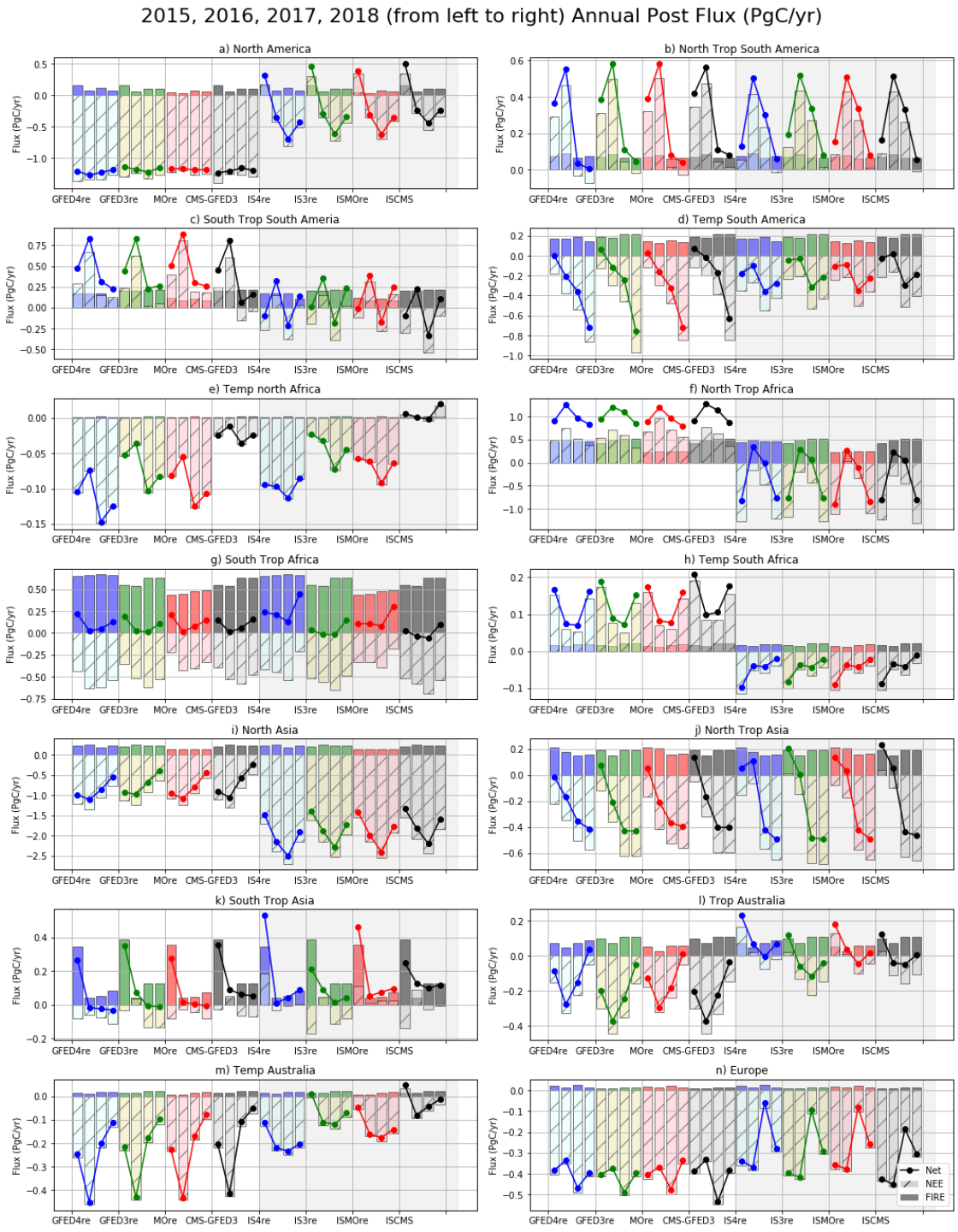

Figure 8. Same as Fig. 7 but for all OCO-2 MIP regions (from left to right, top to bottom) : North America, North Tropical South America, South Tropical South America, Temperate South America, Temperate North Africa, North Tropical Africa, South Tropical Africa, Temperate South Africa, north Asia, North Tropical Asia, South Tropical Asia, Tropical Australia, Temperate Australia, and Europe.

decreases the amount of OCO-2 retrievals, while IS data are located more inside the moist Amazon. This difference in posterior flux could then come from different area of observation. In opposition to the other Southern Tropical regions, the ENSO signal appears in 2016 instead of 2015 for OCO-2. This region follows the inter-seasonal variations of the Northern Tropical regions, which also see highest emissions in 2016.

For Northern Tropical Africa, OCO-2 net fluxes are strong with high sources of carbon between 0.5 PgC/yr and 1.5 PgC/yr. We can see also some fire-dependent differences : FIREMo and FIRE4 sinks decrease for 2017 but FIRE3 driven fluxes do not. This difference in 2017 is particularly observed with OCO-2. IS, on the contrary, give strong sinks in this region, the strongest one for all Tropical regions. Examining Fig. 6, we note the known dependence of the IS posterior emissions with the priors. Northern Tropical Africa is known to have very few IS data compared to the other Tropical regions (Fig. S1). For southern Tropical Africa, we can see the large balance between the fires and the respiration, which are anti-correlated in their variability. GFED4re and MOre have larger sources than GFED3re and CMS-GFED3. With the IS, there is large variation across the priors where IS4re and ISMOre both constrain a source of carbon for the whole period, while ISCMS and IS3re have smaller source of carbon and even a sink in 2016 and 2017. These differences seem to suggest that both fires and respiration are especially important when observational coverage is limited.

Northern Tropical Asia (Fig. 8) shows agreements between the priors and OCO-2 data constraints for 2015 and 2016, but shows significant differences between OCO-2 and IS for 2017 and 2018. The sparse coverage of in-situ data over this region could explain the difference with OCO-2, though not specifically for 2017 alone, and hence further investigations are needed for this region. Finally, for southern Tropical Asia, the inversions adjusted the NEE sinks for MOre and GFED4re to be larger than the two other inversions in order to accommodate the smaller fires observed with FIREMo and FIRE4. This is not observed however for the IS inversions which just show NEE sources for both ISMOre and IS4re. The impact of the fires over this region seems to have a strong impact with both data constraint. If we compare the posteriors with the priors, we can in fact see that the IS tends to be closer to the priors than the OCO-2 inversions. This suggest that for this region as well, the few amount of IS data might explain this result and the larger amount of OCO-2 seems to better constrain the posterior fluxes.

In summary, we observe consistent differences in posterior NEE between IS and OCO-2 inversions. Some of these differences are caused by differences in data coverage and cloud fraction. For all data constraints, we can observe a smaller sinks in the tropics during El Nino, while larger net sinks are observed in the NH Ext. Moreover, larger sinks are observed with OCO-2 in north America and Europe, while larger sinks are observed with IS in Asia. Finally, the net fluxes using FIREMO look like those using FIRE4 for the southern tropical regions, while net fluxes using FIRE3 look alike, suggesting the sensitivity in these regions to the fire prior, not only for IS but also for OCO-2 data constraint.

3.2.3 Evaluation of the simulations

3.2.3.a Evaluation of the inversions to fit the OCO-2 retrievals and IS data

The global distributions of OCO-2 retrievals over the 2015-2018 period (Fig. 9.a) shows a latitudinal gradients from north to south with higher XCO_2 concentrations in the tropics and the northern hemisphere. High land values (no higher than 409 ppm) are observed over east Asia, north west Africa, and north tropical south America. Figure. 9.b shows the global distributions

of IS data with higher number of observations in the northern hemisphere than the tropics or the southern hemisphere. High XCO_2 concentrations (higher than 409 ppm) can be observed for temperate north America and near the coast of east Asia. The regional mean differences between the prior or posterior and the OCO-2 retrievals (IS data) are summarized in Table S1.

The prior have larger differences with the OCO-2 retrievals than the posteriors. The prior3 (using both FIRE3 and NEEre3, see Fig. 2) better fit the OCO-2 measurements than the other priors for the southern hemisphere and the tropics (Fig. 9 and Table S1). The priorCMS however does not fit the OCO-2 measurements with high bias between 3 and 4 ppm. The large difference is also observe with the IS measurements. For the IS inversions, the differences between priors and posteriors with the IS data are very similar. This result suggests that the inversion does not change much from the prior, but this result can be explain due to the small number of observations available in these regions. While the optimized concentrations fit the OCO-2 retrievals quite well compared to the priors, suggesting the inversion's ability to fit the data. For the comparison among the simulations, there is no large difference between the different simulations and the data, particularly for the optimized CO_2 measurements.

3.2.3.b Validation against TCCON data

As mentioned previously, most of the differences observed between in situ and OCO-2 inversions could be due to their respective coverage. in situ measurements have less data over the Tropics and Southern Hemisphere than OCO-2 retrievals. However, besides the spatial coverage, satellite retrievals might be affected, particularly over the Tropics, by the consistently cloudy region known as the Inter-Tropical Convergence Zone (ITCZ) as well as aerosols from biomass burning or dust (such as over and near the Sahara). It is then important to validate the OCO-2 and in situ posterior simulated mixing ratios against independent data. In this section, in order to explore the accuracy in the posterior fluxes, we evaluated the posterior fluxes by sampling the resultant concentrations for comparison with TCCON measurements. All posterior mixing ratios have been sampled around TCCON retrieval locations and times using the appropriate averaging kernels.

In comparison to TCCON, for the 2015-2018 period, the CO posterior biases were underestimated by 7 ppb, while the CO priors were overestimated by 13 ppb (Fig. S10). Even if the posterior biases are lower than the prior biases, the underestimation observed in Fig. S10 against TCCON could explain the low fluxes observed of the FIREMo compared to the other fire estimates over some regions. We can observe an underestimation of the posterior CO mixing ratio of -12 ppb in 2015 at the Ascension Island site, while the a priori CO mixing ratio has an overestimation of 5 ppb in 2015. However, the biases at the Darwin TCCON site give -3 ppb for 2015-2016 (-0.5 ppb for 2017-2018) with the posterior and 20 ppb for 2015-2016 (22 ppb for 2017-2018) with the prior. This gives the impression that our inversion is not getting the best fluxes for Ascension Island, but we can see that this is not the case for other tropical locations. Ascension Island is known to be impacted with Saharan dust and therefore the posterior simulated concentration could be biased due to aerosols.

Figure 10 shows biases between prior and posterior simulated mixing ratio (XCO_2) of the different CO_2 inversions against each TCCON sites. While the priorCMS has the largest biases with TCCON and standard deviation, the other priors used (priorCMS, prior3, prior4, and priorMO) have biases and standard deviation very close each other for most of the sites. Improvements of biases and standard deviation with the prior3 compared to priorCMS, which also use FIRE3 as fire prior, are likely due to the re-balanced respiration that match the NOAA growth rate. This re-balanced respiration and growth rate matches have also been used for prior4 and priorMO. While the re-balanced priors mixing ratio are relatively similar, prior4

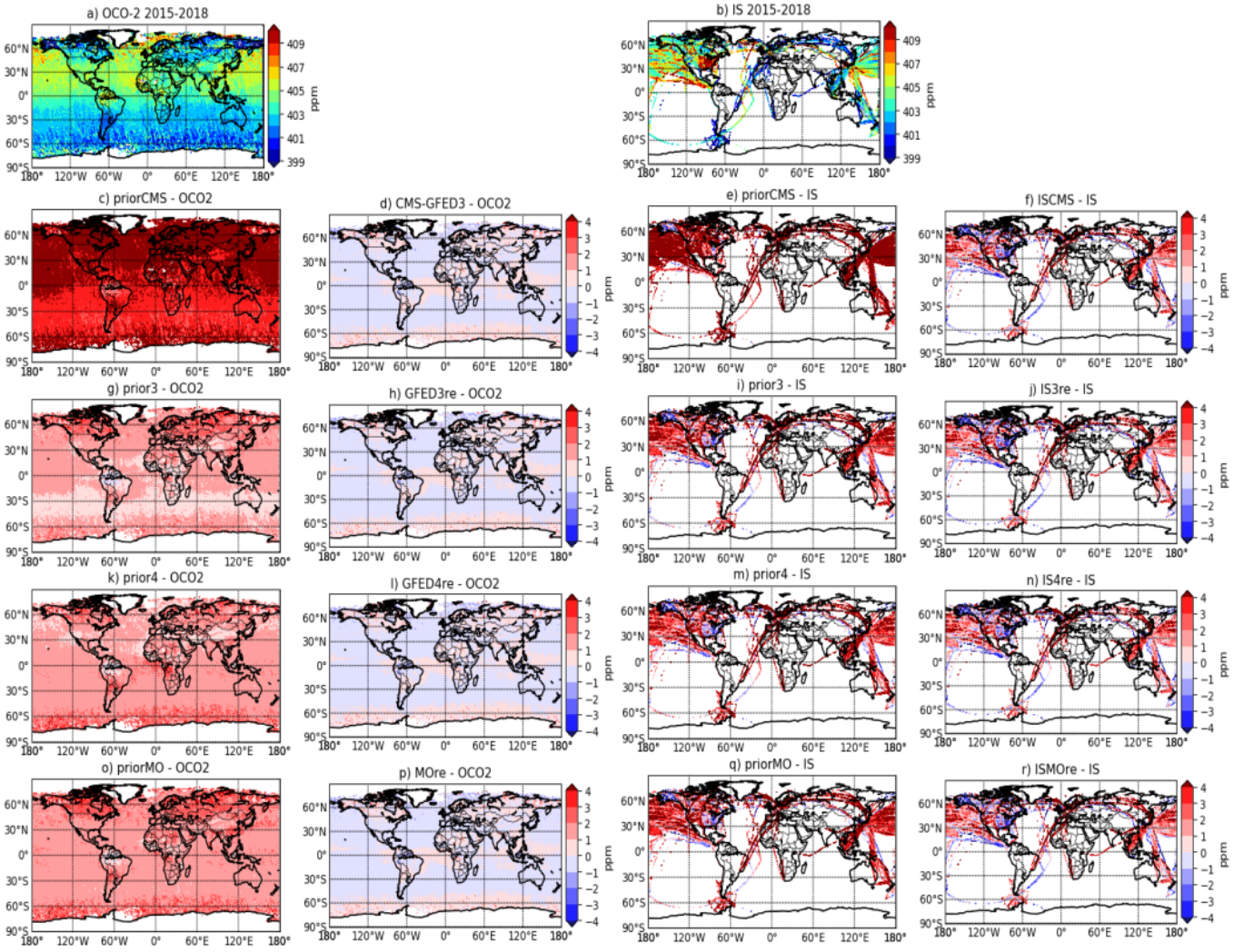

Figure 9. Spatial distributions of the CO_2 total column (XCO_2). Mean distribution of OCO-2 retrieval (a) and In-Situ data (b) over the 2015-2018 period. Annual difference between the prior of each simulation (CMS (2nd row), prior3 (3rd row), prior4 (4th row) and priorMO (5th row)) and OCO-2 in the 1st column (IS in the 3rd column). Annual difference between the posterior simulation of each simulation (row similar to the priors) and OCO-2 in the 2nd column (IS in the 4th column). Results are in ppm.

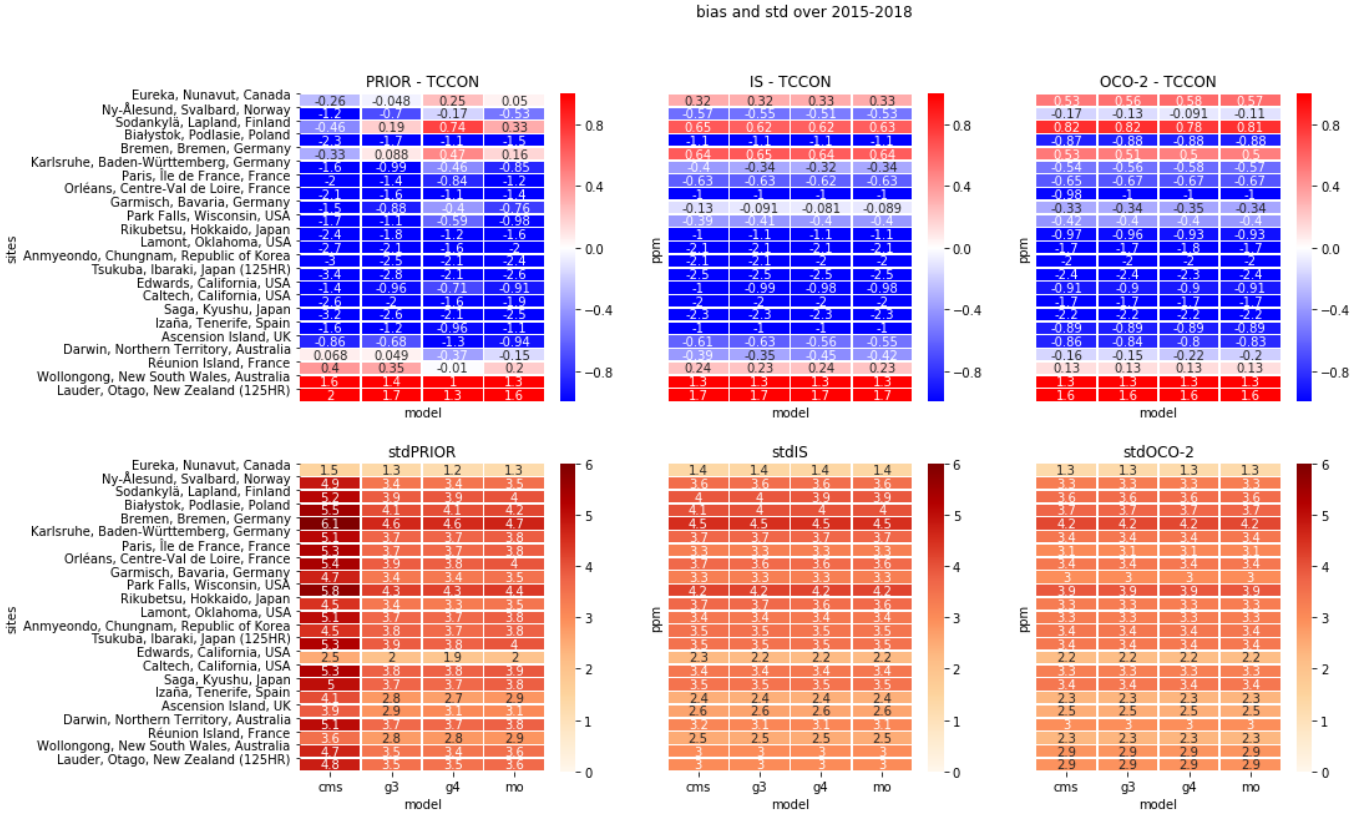

Figure 10. Comparison between TCCON data and the prior (left columns), IS simulations (center columns), and the OCO-2 simulations (right columns). Top panels show experiments biases and bottom panels show standard deviation compared to TCCON sites. Biases and standard deviation are expressed in ppm CO_2. For each panel and from left to right are the simulations CMS, GFED3re, GFED4re and MOre.

and priorMO have less biases than prior3. Additionally, depending on the TCCON site, priorMO bias are slightly lower or smaller than prior4. It is then not straight forward to conclude which re-balanced prior is doing better than the others. The posterior XCO_2 are in better agreement with TCCON measurements than the priors. Biases observed with CMS-GFED3 and ISCMS have been greatly reduced through the inversion, compared to priorCMS, with biases of the same order as compared to the other inversions. For the posterior simulated mixing ratio with IS data, we can see that all biases are very similar among the simulations, and it is here again difficult to conclude which posterior does best. On average, IS4re seems to do better but looking site by site, ISMOre can be better at some tropical sites than the other simulation (such as for Ascension Island and Reunion Island). Same applies for the posterior simulated mixing ratio with OCO-2 data, where there is not one simulation doing better than the others on average. Additionally, all standard deviation are similar between all inversions with slightly larger standard deviation for the IS inversions than for the OCO-2 inversions.

We observed in the results section that posterior fluxes had similarity across the priors used for each data constraint for SH Ext (see Fig. 7) but 2016 is adjusted downward significantly in the OCO-2 fluxes. Evaluation against the two TCCON sites in the SH Ext shows similarity using either IS or OCO-2 constraint (1.3 ppm biases) for Wollongong, but biases are slightly lower with OCO-2 fluxes for Lauder (1.6 ppm with OCO-2 fluxes against 1.7 ppm for IS fluxes). For NH Ext, we observed previously (see Fig. 7 for North America and Europe mainly), a strong sink for OCO-2 over the period compared to IS, which observed stronger year-to-year variability. The evaluation with TCCON data at European sites, shows smaller biases using IS data than OCO-2 data for all simulations. For instance at Garmisch site, biases are around -0.1 ppm and -0.34 ppm with IS fluxes and OCO-2 fluxes respectively, showing a larger underestimation with OCO-2 than IS fluxes. But for the northern American sites, biases are lower with OCO-2 fluxes than IS fluxes (see Lamont site for instance in Fig. 10).

4 Discussion

In this study, we have presented an optimized CO_2 fire prior flux based on emission ratio between CO_2 and CO that comes from optimized CO fire emissions using MOPITT CO retrievals. In addition, as fire emissions and plant respiration (terms included in the net fluxes) are difficult to disentangle, we re-balanced the respiration with each fire prior and with the annual NOAA growth rate. We then explored a range of NEE emissions based on different fire emissions including a CO_2 fire estimate calculated from CO fire emissions information in order to better constrain biospheric emissions. We focused our study for the period 2015-2018 to observe the impact of the El Niño event in 2015 and the recovery period which followed it.

Globally, and for most regions, we find that the dependence of the inversion results on prior emissions is of secondary importance when compared with the data constraint, in the sense that variations in posterior flux are much smaller across different prior mean fluxes (and the different uncertainties that come from scaling the prior mean flux) as compared with differences resulting from assimilating OCO-2 versus in situ data. There are exceptions, most notably in the Northern and Southern Tropics, where the in situ constraint is especially limited and the corresponding posterior annual fluxes vary by as much as 0.5 PgC, which is a large fraction of the expected total El Niño signal. This suggests that in situ constrained flux estimates in the Tropics are more sensitive to the assumed prior flux, of which fires are a significant component, and should be assigned the appropriate amount of uncertainty in accordance with this finding. It also implies that while residual biases in satellite retrievals remain a key focus of the top-down inversion community, further work is needed to improve prior fluxes in Tropical regions as well as deploy more in situ measurements. Current efforts by multiple organizations should assist in that effort on a short time basis, but more investments in long term monitoring are needed (communication from Kathryn McKain). OCO-2 inversions are also sensitive to the prior assumption in Northern Africa, though to a lesser extent, as well as in Tropical Asia. Tropical Asia have been particularly well studied in the past where Nechita-banda et al. (2018) and van der Werf et al. (2017) have shown the underestimation of GFED inventories over peat fires compared to space-based instruments such as IASI and MOPITT. This reinforces the need for better measurements and bottom up estimates of biospheric and fire fluxes in these Tropical regions. Nechita-Banda et al. (2018) converted their CO fire emissions in CO_2 emissions using emission factors and estimated that a range of 0.35-0.60 PgC was emitted in Indonesia and Papua from the 2015 fires. We calculated our fire CO_2

emissions over the same region and found 0.41 PgC, 0.37 PgC and 0.39 PgC for FIRE3, FIRE4 and FIREMo respectively. Our fire CO_2 estimates are hence in agreement with those found by Nechita-Banda et al. (2018). As mentioned previously, we know that GFED4.1s has information of small fires compared to GFED3 which allow better accuracy particularly over the Tropics where peat fires are important. However, we can see lower FIRE4 emissions than FIRE3 for southern tropical south Asia, similarly to what Shi et al. (2015) have found for the 2002-2012 period. A possible explanation could be that the CASA biogeochemical model of GFED3 predicts higher biomass densities than with the new version used in GFED4. Validation against fuel loads measured in savanna and grassland field have been found higher than with GFED4 (Randerson et al., 2012; Giglio et al., 2013). In 2015, during the onset of the El Niño event which caused intense fires over Indonesia, FIREMo emissions are stronger than with FIRE4 emissions but lower than FIRE3 emissions. Fires over peat lands spread more during the El Niño event due to intense drought conditions (Nechita-Banda et al., 2018). Consequently, they emit two to four times more CO than forest fires (Akagi et al., 2011) and contribute significantly to the exchange between terrestrial carbon stocks and the atmosphere by decreasing the uptake of atmospheric CO_2 by the biosphere. This is particularly shown for the IS inversions where IS4re and ISMOre have higher net sources of carbons compared to the IS constrained with GFED3 fires. Moreover, FIREMo was able to catch the seasonality of fires over southern tropical Asia during the El Niño event, compared to the other priors using GFED inventory. As discussed in Nechita-Banda et al. (2018) and van der Laan-Luijkx et al. (2015) for Equatorial Asia and tropical south America, GFED4 does not capture fire seasonality due to the use of burned area, compared to GFAS. In both GFED and GFAS method (and similarly for MOPITT), the detection of fires underneath clouds and below the canopy is difficult. But, FIREMo emissions, compared to FIRE3 and FIRE4, has the advantage of combining optimized fire emissions with local observations. It is thus important to use CO observations to constrain estimates of CO_2 fire emissions, and subsequently constrain NEE with OCO-2 and IS observations But uncertainty in our emission ratio remains when converting CO to CO_2 emissions in our prior. GFED vegetation partition only account for six different types of vegetation which might not be fine enough to represent all different types of fuels. Additionally, the emission factors, used in the emission ratio, lack spatial and temporal variability to account for the full dynamics range of combustion characteristics. We know, for instance, that African savanna fires can go from flaming to smoldering, changing the combustion efficiency and then the gases emitted (Zheng et al., 2018b). This could explain the differences observed over some regions of the Tropics between FIREMo and the other prior fire CO_2 emissions. Further works is required to improve emission ratios and particularly emission factors over different spatial and temporal scales. A recent study has shown the underestimation for Africa of MODIS burned area and consequently GFED4s, compared to the new Sentinel-2 burned area product (Ramo et al., 2021). The higher fire posterior emissions observed with previous studies using GFAS as a prior compared to GFED4 (Nechita-banda et al., 2018) and the results of Ramo et al. (2021) seems to suggest for future work to carefully choose the CO fire prior used in a CO-CO_2 study. Future work will be done comparing different CO posterior emissions.

However, the estimation of EF and consequently the emission ratio CO/CO_2 cannot be determined accurately in the field and can introduce systematic errors in the EF(CO_2) values that may well exceed 10%. One challenge is separation of the information between small fire inputs of CO_2 (and hence their detection) from large biospheric variability. Other difficulties

come from the issue of variable background concentrations and from smoldering emissions that are not projected into the smoke plumes (Guyon et al., 2005; Burling et al., 2011; Yokelson et al., 2013).

The data used to constrain inversions is very important. We could see up to 0.4 PgC/yr differences between OCO-2 and IS inversions in tropical regions. This bring us to the importance of the data assimilated in the inversions but also about the priors used in the inversions concerning the different sectors (fire and terrestrial emissions).

The difference in partitioning of fluxes in latitude and longitude for the different data constraints is not a new observation, and fits the findings of the v7 OCO-2 MIP Crowell et al. (2019) and previous studies comparing GOSAT and in situ data (Reuter et al., 2014; Houweling et al., 2015)) as well as of the v9 OCO-2 MIP, an extension of the v7 OCO-2 MIP (Peiro et al., 2022). More specifically, the OCO-2 data constrain a stronger Northern Extra-Tropical sink in concert with a strong tropical source, while the in situ data generally constrain a weaker Northern sink and neutral Tropical flux, or even a sink. While the Northern Extra-Tropics are relatively densely sampled by the in situ network, Schuh et al. (2019) found a strong sensitivity of flux estimates to model transport, particularly in the vertical and meridional transport of CO_2. Though we utilized only TM5 in these experiments, the findings here are consistent with those found in their study.

Regarding the question of the importance of the prior and the question of which prior could do better than the others, we have seen through the results and the evaluation, than no simulation is better than the other on average. Even if the biases seem to have been reduced with FIREMo for certain sites (such as Ascension island for instance), they are in the same order as the other a priori biases for other site. On average and overall, the added value of optimizing fire emissions before optimizing NEE is not very apparent. Our results seem, overall, to be very insensitive to optimized fire emissions. Philip et al. (2019) performed simulation experiments with different NEE priors, and concluded that posterior NEE estimates are insensitive to prior flux values. But they found large spread among posterior NEE estimates in regions with limited OCO-2 observations. Our results suggesting that OCO-2 inversions are relatively insensitive to prior in most regions, are consistent with Philip et al. (2019), and not only for OCO-2 inversions but also for IS inversions.

A generally accepted (though not documented) assertion is that a minimal amount of data is required to constrain the global growth rate, and yet we see here that OCO-2 and the global in situ network do not see the same global annual flux, even assuming the same transport and prior flux that matches the NOAA AGR. Part of this discrepancy is certainly due to: (i) most of the in situ measurements assimilated here are taken in the atmospheric boundary layer while OCO-2 represents a column density; and (ii) most of the in situ measurements are in the northern extra-tropics, whereas OCO-2 measurements are globally distributed, but with seasonally varying coverage. Persistent transport biases as well as satellite retrieval errors likely play a factor in this global offset, though further investigation is necessary to assess the relative importance of each.

5 Conclusions

In this study, we have explored the potential of using CO/CO_2 emission ratio to add CO fire information in CO_2 inversions in order to better estimate and constrain CO_2 biospheric emissions. Fires have the potential to influence inter-annual variability and long-term trends in atmospheric CO_2 concentrations and particularly alter the seasonal cycle of net biome production. CO

measurements are available with high precision from space and bring more accuracy in CO fire emission estimates. Including more accurate fire emissions in CO_2 inversions could improve the estimates of CO_2 land fluxes relative to a CO_2 inversion without the added information of CO. In this paper, we showed how we added on global scale CO/CO_2 emission ratio and its respective re-balanced respiration with fire and NEE with annual NOAA growth rate, and its value for CO_2 inversions.

We performed several CO_2 transport inversions assimilating separately OCO-2 data and in situ measurements from 2015 through 2018. We found that OCO-2 and in situ net fluxes have, even if with a difference, a better agreement at global scale as observations are dense enough to constrain the fluxes than at latitudinal and regional scale. Differences in net fluxes are particularly important over the Tropics not only between OCO-2 and in situ inversions but also between the different priors used. Discrepancies between in situ and OCO-2 inversions occurred over Northern Tropical Africa where OCO-2 inversions have shown net sources while in situ inversions have shown sinks. However, over Southern Tropical regions, discrepancies appear between the different set of priors, with higher net sources observed with the inversion using the CO/CO_2 emission ratio (MOre inversion) for OCO-2 inversion over Southern Tropical South America and with IS inversion over Southern Tropical Asia, compared to the IS inversions using GFED3 fires. For tropical Asia, the constrain of priors seems to be more important than the data assimilated. Additionally, over this region, seasonality from CO_2 inversions using MOPITT fires seems to be better representative of the large Indonesian fires that occurred during the 2015 El Niño event.

TCCON evaluation suggested that the prior using the FIREMo (CO_2 fire prior emissions computing using CO/CO_2 emission ratio) gives accuracy in CO_2 mixing ratio comparable to GFED4 but with slightly larger biases over the Northern Hemisphere and biases of the priors with the re-balanced respiration are smaller than the CMS prior. However, biases for the posterior simulated mixing ratio are in the same order. Evaluation mainly showed that biases have been decreased and variability matches better those of TCCON for the re-balanced posterior simulated mixing ratio suggesting the importance of the accuracy in fire priors and the re-balanced of terrestrial emission with fires for CO_2 posteriors emissions. The added value of fire emission for NEE optimization is not apparent. Our results seem hence to be very insensitive to optimized fire emissions.

We illustrated the potential of using CO/CO_2 emission ratio, and the re-balanced respiration and NEE with fire and growth rate, in CO_2 inversion for better constraint and accuracy in the CO_2 fire prior emissions and biospheric emission estimates. We found that CO_2 fluxes are more robust if the NEE and fire emissions are rebalanced in order to match the NOAA AGR. However, a more reliable NEE is obtained with the assimilated data, using either in situ or satellite-based CO_2 constraints. This opens new avenues for future research for the development of a joint CO-CO_2 inversion framework that uses multiple streams of data to improve the fire and biosphere emissions. Besides, the multi-species approach employing CO and CO_2 for instance is important for the interpretation of upcoming satellite data such as data from the future NASA Earth Venture Mission, GeoCarb.

Appendix A: GFED versions descriptions

The first version of GFED was released in 2004. Since then, several improvements have been incorporated into GFED. Improvement on the mapping of burned area from active fire data in GFED2 (Giglio et al., 2006) was no longer necessary when the MODIS product became available for GFED3 (Giglio et al., 2009). Burned area particularly affects the spatiotemporal variability of carbon emissions during fires. This spatiotemporal impact has been implemented in GFED with biogeochemical modeling framework providing estimation of biomass combustion over different vegetation types (Giglio et al., 2013). All GFED versions are then based on the Carnegie-Ames-Standford Approach (CASA) model adjusted to account for fires (see van der Werf et al. (2004) and van der Werf et al. (2017) for more details). The most recent versions (GFED4 and GFED4.1s which includes small fire burned area) modified the burned-area-to-burned fraction conversion, which have been shown to increase burned area and fire carbon emissions with 11% in GFED4.1s compared to GFED3 (van der Werf et al., 2017) at the global scale. Liu et al. (2017b) found that with the omission of small fires in GFED3, global fire emissions are underestimated. Accounting for small fires increased global burned area and carbon emissions by 35% (Randerson et al., 2012), and improved the agreement of spatial distribution between active fires and burned area over regions with large fires such as savanna fires and boreal forests. Including small fires in GFED amplifies emissions over regions where drought stress and burned area varied considerably from year to year in response to, for instance, the El Niño Southern Oscillation (ENSO).

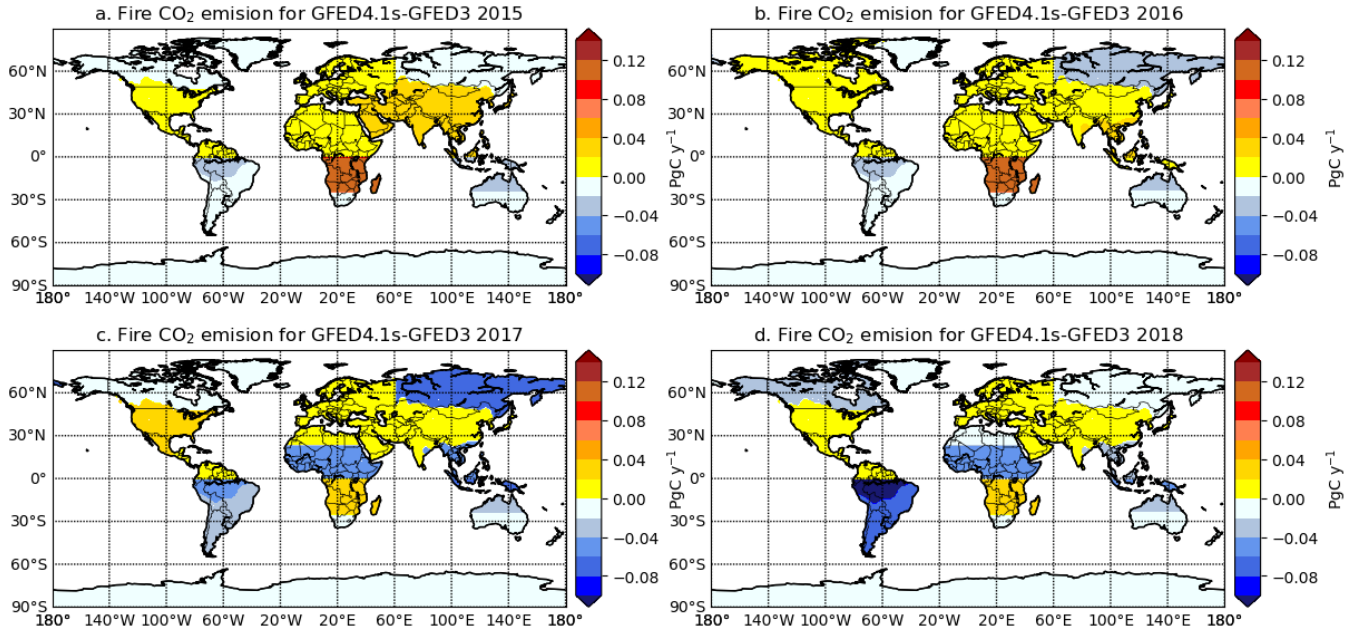

Figure A1. Annual differences between FIRE4 and FIRE3 in PgC/yr over the regions of Fig. 3 for a) 2015, b) 2016, c) 2017 and d) 2018.

Figure A1 shows annual differences between FIRE3 and FIRE4 from 2015 through 2018 over the OCO-2 MIP regions. We note that regional differences are as large as 140 TgC per year, or roughly ∼10% of the annual global fire emissions budget

which has been estimated to 1.6 $\pm$ 0.7 GtC/yr (Friedlingstein et al., 2020). Additionally, the size and sign of the differences varies by year and by region. For instance, FIRE3 generally predicts higher CO_2 emissions over the Boreal regions, while FIRE4 (GFED4.1s) largely predicts more fire emissions from the Northern midlatitudes. This is consistent with differences between the two models, i.e. GFED4.1s uses a different set of emission factors separating trace gas emissions and aerosol from boreal forest to temperate forests (Akagi et al., 2011; van der Werf et al., 2017). van der Werf et al. (2017) have shown that GFED3 does not capture the different patterns of fire severity between the boreal regions of North America and Eurasia and the differences between boreal and temperate forests fires (which could explain the large difference between FIRE4 and FIRE3 in Fig.A1). In addition, van der Werf et al. (2017) found that including small fire burned area in GFED4 doubled the burned area in temperate North America and Europe compared to GFED3. Interestingly, the differences in the tropics have a pronounced zonal structure, where GFED4.1s predicts smaller emissions in south America, tropical Asia, and north Africa (after 2016), and larger emissions in southern tropical Africa. The addition of small fire burned area included in GFED4.1s has a strong impact in the southern tropical Africa regions where agricultural waste burning and shifting cultivation are important drivers of fire activity. van der Werf et al. (2017) have shown that the increase of burned area in these regions were associated with small fire burned area from the last GFED version. Small fires linked with deforestation and agricultural waste are also important over the Indonesia, however deforestation activity decreased of almost 50% in 2017 and 2018 thanks to several Indonesian policies in order to prevent forest fires and land clearing with particularly the new law avoiding to clear forest for oil palm plantations (Global Forest Watch, 2020). This might explain the decrease in fire emissions over Southern Tropical Asia in 2017 and 2018 with GFED4.1s, in addition that 2017 and 2018 were not impacted by the 2015 El Niño event where large fires burned in Indonesia.

Author contributions. H.Peiro generated the CO products, MOPITT CO_2 fires and re-balanced priors, produced the figures and wrote the manuscript. S.Crowell generated the CO_2 products, provided comments and feedback on the manuscript. B.Moore provided feedback on the manuscript as well.

Competing interests. The authors declare that they have no conflict of interest.

Acknowledgements. We are thankful to Debra Wunch who helped us reviewing the TCCON references and acknowledgements, and to both Debra Wunch and Coleen Roehl who contacted the TCCON PIs. The TCCON data were obtained from the TCCON Data Archive hosted by CaltechDATA at https://tccondata.org. We thanks TCCON PIs for the TCCON measurements at Eureka, Ny-Ålesund, Sodankylä, Białystok, Bremen, Karlsruhe, Paris, Orléans, Garmisch, Park Falls, Rikubetsu, Lamont, Anmeyondo, Tsukuba, Edwards, Caltech, Saga, Izaña, Ascension Island, Darwin, Réunion Island, Wollongong, Lauder. Eureka measurements are made by the Canadian Network for the Detection of Atmospheric Change (CANDAC) and in part by the Canadian Arctic ACE Validation Campaigns. They are supported by the Atlantic Innovation Fund/Nova Scotia Research Innovation Trust, Canada Foundation for Innovation, Canadian Foundation for Climate and Atmospheric Sciences, Canadian Space Agency, Environment Canada, Government of Canada International Polar Year funding, Natural Sciences and Engineering Research Council, Northern Scientific Training Program, Ontario Innovation Trust, Ontario Research Fund and Polar Continental Shelf Program. Observations for Białystok are funded byt the European Union (EU) projects InGOS and ICOS-INWIRE, and bu the Senate of Bremen. Local support for Bremen and Ny-Ålesund are provided by the EU projects InGOS and ICOS-INWIRE (26188, 36677, 284274, 313169 and 640276), and by the Senate of Bremen. Orléans observations are supported by the EU projects InGOS and ICOS-INWIRE, by the Senate of Bremen and by the RAMCES team at LSCE. The Réunion Island TCCON site is operated by the Royal Belgian Institute for Space Aeronomy with financial support since 2014 by the EU project ICOS-Inwire and the ministerial decree for ICOS (FR/35/IC1 to FR/35/IC5) and local activities supported by LACy/UMR8105 – Université de La Réunion. The Paris TCCON site has received funding from Sorbonne Université, the French research center CNRS, the French space agency CNES, and Région Île-de-France. Garmisch funding was provided by the EC within the INGOS project. Park Falls, Lamont, Edwards and Caltech TCCON site have received funding from National Aeronautics and Space Administration (NASA) grants NNX14AI60G, NNX11AG01G, NAG5-12247, NNG05-GD07G, and NASA Orbiting Carbon Observatory Program. They are supported in part by the OCO-2 project. The TCCON station at Rikubetsu and Tsukuba are supported in part by the GOSAT series project. Darwin and Wollongong TCCON stations are funded by NASA grants NAG5-12247 and NNG05-GD07G and supported by the Australian Research Council (ARC) grants DP140101552, DP110103118, DP0879468 and LP0562346. Lauder TCCON site has received funding from National Institute of Water and Atmospheric (NIWA) Research through New Zealand's Ministry of Business, Innovation and Employment. We also acknowledge the ObsPack data used for our IS inversions. The computing for this project was performed at the OU Supercomputing Center for Education Research (OSCER) at the University of Oklahoma (OU). The authors also thank Sourish Basu and John Miller for the development of the CO inversion capability in TM5 4DVAR (https://sourceforge.net/p/tm5/cy3_4dvar/ci/default/tree/) used in this work. The CO inversion methodology was developed under the NASA Carbon Monitoring System program, Interagency agreement NNH16AD06I.

References

Akagi, S. K., Yokelson, R. J., Wiedinmyer, C., Alvarado, M. J., Reid, J. S., Karl, T., Crounse, J. D., and Wennberg, P. O.: Emission factors for open and domestic biomass burning for use in atmospheric models, Atmospheric Chemistry and Physics, 11, 4039–4072, https://doi.org/10.5194/acp-11-4039-2011, 2011.

Andreae, M. and Merlet, P.: Emission of trace gases and aerosols from biomass burning, Global Biogeochemical Cycles, 15, 955–966, 2001.

Andreae, M. O.: Emission of trace gases and aerosols from biomass burning – An updated assessment, Atmospheric Chemistry and Physics Discussions, pp. 1–27, https://doi.org/10.5194/acp-2019-303, https://www.atmos-chem-phys-discuss.net/acp-2019-303/, 2019.

Arellano, A. F., Kasibhatla, P. S., Giglio, L., van der Werf, G. R., and Randerson, J. T.: Top-down estimates of global CO sources using MOPITT measurements, Geophysical Research Letters, 31, 1–5, https://doi.org/10.1029/2003GL018609, 2004.

Atkinson, R.: Atmospheric chemistry of VOCs and NOx, Atmospheric Environment, 34, 2063–2101, 2000.

Aumann, H. H., Chahine, M. T., Gautier, C., Goldberg, M. D., Kalnay, E., McMillin, L. M., Revercomb, H., Rosenkranz, P. W., Smith, W. L., Staelin, D. H., Strow, L. L., and Susskind, J.: AIRS/AMSU/HSB on the aqua mission: design, science objectives, data products, and processing systems, IEEE Transactions on Geoscience and Remote Sensing, 41, 253–264, https://doi.org/10.1109/TGRS.2002.808356, 2003.

Baker, D. F., Doney, S. C., and Schimel, D. S.: Variational data assimilation for atmospheric CO2, Tellus, Series B: Chemical and Physical Meteorology, 58, 359–365, https://doi.org/10.1111/j.1600-0889.2006.00218.x, 2006.

Baker, D. F., Bösch, H., Doney, S. C., O'Brien, D., and Schimel, D. S.: Carbon source/sink information provided by column CO2 measurements from the Orbiting Carbon Observatory, Atmospheric Chemistry and Physics, 10, 4145–4165, https://doi.org/10.5194/acp-10-4145-2010, 2010.

Bakwin, P. S., D.F., H., P.P., T., and J.W., E.: Anthropogenic sources of halocarbons , sulfur hexafluoride , carbon monoxide , and methane in the southeastern United States, Journal of Geophysical Research, 102, 915–925, 1997.

Baldassarre, G., Pozzoli, L., Schmidt, C. C., Unal, A., Kindap, T., Menzel, W. P., Whitburn, S., Coheur, P. F., Kavgaci, A., and Kaiser, J. W.: Using SEVIRI fire observations to drive smoke plumes in the CMAQ air quality model: A case study over Antalya in 2008, Atmospheric Chemistry and Physics, 15, 8539–8558, https://doi.org/10.5194/acp-15-8539-2015, 2015.

Ballantyne, A. P., Alden, C. B., Miller, J. B., Trans, P. P., and White, J. W.: A Newtonian approach to extraordinarily strong negative refraction, Nature, 488, 70–73, https://doi.org/10.1038/nature11299, 2012.

Bastos, A., Friedlingstein, P., Sitch, S., Chen, C., Mialon, A., Wigneron, J. P., Arora, V. K., Briggs, P. R., Canadell, J. G., Ciais, P., Chevallier, F., Cheng, L., Delire, C., Haverd, V., Jain, A. K., Joos, F., Kato, E., Lienert, S., Lombardozzi, D., Melton, J. R., Myneni, R., Nabel, J. E., Pongratz, J., Poulter, B., Rödenbeck, C., Séférian, R., Tian, H., Van Eck, C., Viovy, N., Vuichard, N., Walker, A. P., Wiltshire, A., Yang, J., Zaehle, S., Zeng, N., and Zhu, D.: Impact of the 2015/2016 El Niño on the terrestrial carbon cycle constrained by bottom-up and top-down approaches, Philosophical Transactions of the Royal Society B: Biological Sciences, 373, https://doi.org/10.1098/rstb.2017.0304, 2018.

Basu, S., Guerlet, S., Butz, A., Houweling, S., Hasekamp, O., Aben, I., Krummel, P., Steele, P., Langenfelds, R., Torn, M., Biraud, S., Stephens, B., Andrews, A., and Worthy, D.: Global CO2 fluxes estimated from GOSAT retrievals of total column CO2, Atmospheric Chemistry and Physics, 13, 8695–8717, https://doi.org/10.5194/acp-13-8695-2013, 2013.

Basu, S., Krol, M., Butz, A., Clerbaux, C., Sawa, Y., Machida, T., Matsueda, H., Frankenberg, C., Hasekamp, O. P., and Aben, I.: The seasonal variation of the CO2 flux over Tropical Asia estimated from GOSAT, CONTRAIL, and IASI, Geophysical Research Letters, 41, 1809–1815, https://doi.org/10.1002/2013GL059105, 2014.

Basu, S., Baker, D. F., Chevallier, F., Patra, P. K., Liu, J., and Miller, J. B.: The Impact of Transport Model Differences on CO 2 Surface Flux Estimates from OCO-2 Retrievals of Column Average CO 2, 20, 1–32, https://doi.org/10.5194/acp-18-7189-2018, 2018.

Beer, R.: TES Scientific Objectives & Approach, Goals & Requirements, Jet Propulsion Laboratory, California Institue of Technology, D-11294, 1999.

Blumenstock, T., Hase, F., Schneider, M., García, O. E., and Sepúlveda, E.: TCCON data from Izana (ES), Release GGG2014.R1, https://doi.org/10.14291/TCCON.GGG2014.IZANA01.R1, https://data.caltech.edu/records/302, 2017.

Burling, I. R., Yokelson, R. J., Akagi, S. K., Urbanski, S. P., Wold, C. E., Griffith, D. W., Johnson, T. J., Reardon, J., and Weise, D. R.: Airborne and ground-based measurements of the trace gases and particles emitted by prescribed fires in the United States, Atmospheric Chemistry and Physics, 11, 12 197–12 216, https://doi.org/10.5194/acp-11-12197-2011, 2011.

Byrne, B., Jones, D. B., Strong, K., Zeng, Z. C., Deng, F., and Liu, J.: Sensitivity of CO2 surface flux constraints to observational coverage, Journal of Geophysical Research, 122, 6672–6694, https://doi.org/10.1002/2016JD026164, 2017.

Chevallier, F., Engelen, R. J., and Peylin, P.: The contribution of AIRS data to the estimation of CO2 sources and sinks, Geophysical Research Letters, 32, 1–4, https://doi.org/10.1029/2005GL024229, 2005.

Clerbaux, C., Boynard, A., Clarisse, L., George, M., Hadji-Lazaro, J., Herbin, H., Hurtmans, D., Pommier, M., Razavi, A., Turquety, S., Wespes, C., and Coheur, P.-F.: Monitoring of atmospheric composition using the thermal infrared IASI/MetOp sounder, Atmospheric Chemistry and Physics, 9, 6041–6054, https://doi.org/10.5194/acp-9-6041-2009, 2009.

Cooperative Global Atmospheric Data Integration Project: Multi-laboratory compilation of atmospheric carbon dioxide data for the period 1957-2018; {obspack_co2_1_GLOBALVIEWplus_v5.0_2019_08_12}, https://doi.org/10.25925/20190812, 2019.

Crisp, D. and Johnson, C.: The orbiting carbon observatory mission, Acta Astronautica, 56, 193–197, https://doi.org/10.1016/j.actaastro.2004.09.032, 2005.

Crisp, D., Fisher, B. M., O'Dell, C., Frankenberg, C., Basilio, R., Bösch, H., Brown, L. R., Castano, R., Connor, B., Deutscher, N. M., Eldering, A., Griffith, D., Gunson, M., Kuze, A., Mandrake, L., McDuffie, J., Messerschmidt, J., Miller, C. E., Morino, I., Natraj, V., Notholt, J., O'Brien, D. M., Oyafuso, F., Polonsky, I., Robinson, J., Salawitch, R., Sherlock, V., Smyth, M., Suto, H., Taylor, T. E., Thompson, D. R., Wennberg, P. O., Wunch, D., and Yung, Y. L.: The ACOS CO 2 retrieval algorithm - Part II: Global X CO2 data characterization, Atmospheric Measurement Techniques, 5, 687–707, https://doi.org/10.5194/amt-5-687-2012, 2012.

Crisp, D., Pollock, H., Rosenberg, R., Chapsky, L., Lee, R., Oyafuso, F., Frankenberg, C., Dell, C., Bruegge, C., Doran, G., Eldering, A., Fisher, B., Fu, D., Gunson, M., Mandrake, L., Osterman, G., Schwandner, F., Sun, K., Taylor, T., Wennberg, P., and Wunch, D.: The on-orbit performance of the Orbiting Carbon Observatory-2 (OCO-2) instrument and its radiometrically calibrated products, Atmospheric Measurement Techniques, 10, 59–81, https://doi.org/10.5194/amt-10-59-2017, 2017.

Crowell, S., Baker, D., Schuh, A., Basu, S., Eldering, A., Feng, L., Crisp, D., O'Dell, C., Liu, J., Jacobson, A. R., Chatterjee, A., McKain, K., Schimel, D., Sweeney, C., Oda, T., Palmer, P. I., Nassar, R., Deng, F., Jones, D. B., Miller, J., Stephens, B., and Chevallier, F.: The 2015-2016 Carbon Cycle As Seen from OCO-2 and the Global In Situ Network, Atmospheric Chemistry and Physics Discussions, pp. 1–79, https://doi.org/10.5194/acp-2019-87, 2019.

Crowell, S. M., Randolph Kawa, S., Browell, E. V., Hammerling, D. M., Moore, B., Schaefer, K., and Doney, S. C.: On the Ability of Space-Based Passive and Active Remote Sensing Observations of CO2to Detect Flux Perturbations to the Carbon Cycle, Journal of Geophysical Research: Atmospheres, 123, 1460–1477, https://doi.org/10.1002/2017JD027836, 2018.

Darmenov, A. S. and Silva, A.: The Quick Fire Emissions Dataset (QFED): Documentation of versions 2.1, 2.2 and 2.4, NASA Technical Report Series on Global Modeling and Data Assimilation, NASA/TM-2015-104606, 38, 2015.

De Mazière, M., Sha, M. K., Desmet, F., Hermans, C., Scolas, F., Kumps, N., Metzger, J.-M., Duflot, V., and Cammas, J.-P.: TCCON data from Réunion Island (RE), Release GGG2014.R1, https://doi.org/10.14291/TCCON.GGG2014.REUNION01.R1, https://data.caltech.edu/records/322, 2017.

Dee, D. P., Uppala, S. M., Simmons, A. J., Berrisford, P., Poli, P., Kobayashi, S., Andrae, U., Balmaseda, M. A., Balsamo, G., Bauer, P., Bechtold, P., Beljaars, A. C., van de Berg, L., Bidlot, J., Bormann, N., Delsol, C., Dragani, R., Fuentes, M., Geer, A. J., Haimberger, L., Healy, S. B., Hersbach, H., Hólm, E. V., Isaksen, L., Kållberg, P., Köhler, M., Matricardi, M., Mcnally, A. P., Monge-Sanz, B. M., Morcrette, J. J., Park, B. K., Peubey, C., de Rosnay, P., Tavolato, C., Thépaut, J. N., and Vitart, F.: The ERA-Interim reanalysis: Configuration and performance of the data assimilation system, Quarterly Journal of the Royal Meteorological Society, 137, 553–597, https://doi.org/10.1002/qj.828, 2011.

Deeter, M. N., Emmons, L. K., Francis, G. L., Edwards, D. P., Gille, J. C., Warner, J. X., Khattatov, B., Ziskin, D., Lamarque, J. F., Ho, S. P., Yudin, V., Attié, J. L., Packman, D., Chen, J., Mao, D., and Drummond, J. R.: Operational carbon monoxide retrieval algorithm and selected results for the MOPITT instrument, Journal of Geophysical Research D: Atmospheres, 108, 1–11, https://doi.org/10.1029/2002jd003186, 2003.

Deeter, M. N., Edwards, D. P., Gille, J. C., and Drummond, J. R.: Sensitivity of MOPITT observations to carbon monoxide in the lower troposphere, Journal of Geophysical Research Atmospheres, 112, 1–9, https://doi.org/10.1029/2007JD008929, 2007.

Deeter, M. N., Edwards, D. P., GIIIe, J. C., and Drummond, J. R.: CO retrievals based on MOPITT near-infrared observations, Journal of Geophysical Research Atmospheres, 114, 1–9, https://doi.org/10.1029/2008JD010872, 2009.

Deeter, M. N., Martínez-Alonso, S., Edwards, D. P., Emmons, L. K., Gille, J. C., Worden, H. M., Pittman, J. V., Daube, B. C., and Wofsy, S. C.: Validation of MOPITT Version 5 thermal-infrared, near-infrared, and multispectral carbon monoxide profile retrievals for 2000-2011, Journal of Geophysical Research Atmospheres, 118, 6710–6725, https://doi.org/10.1002/jgrd.50272, 2013.

Deeter, M. N., Edwards, D. P., Gille, J. C., and Worden, H. M.: Information content of MOPITT CO profile retrievals: Temporal and geographical variability, Journal of Geophysical Research, 120, 12,723–12,738, https://doi.org/10.1002/2015JD024024, 2015.

Deeter, M. N., Edwards, D. P., Francis, G. L., Gille, J. C., Mao, D., Martinez-Alonso, S., Worden, H. M., Ziskin, D., and Andreae, M. O.: Radiance-based Retrieval Bias Mitigation for the MOPITT Instrument: The Version 8 Product, Atmospheric Measurement Techniques Discussions, pp. 1–30, https://doi.org/10.5194/amt-2019-41, 2019.

Deutscher, N. M., Notholt, J., Messerschmidt, J., Weinzierl, C., Warneke, T., Petri, C., and Grupe, P.: TCCON data from Bialystok (PL), Release GGG2014.R2, https://doi.org/10.14291/TCCON.GGG2014.BIALYSTOK01.R2, https://data.caltech.edu/records/1300, 2019.

Drummond, J. R.: Measurements of pollution in the tropopshere (MOPITT) instrument, Sensor Systems for the Early Earth Observing System Platforms, 1939, 126–136, https://doi.org/10.1117/12.152839, 1993.

Drummond, J. R., Zou, J., Nichitiu, F., Kar, J., Deschambaut, R., and Hackett, J.: A review of 9-year performance and operation of the MOPITT instrument, Advances in Space Research, 45, 760–774, https://doi.org/10.1016/j.asr.2009.11.019, http://dx.doi.org/10.1016/j.asr.2009.11.019, 2010.

Drummond, J. R., Hackett, J., and Caldwell, D.: Measurements ofpollution in the troposphere (MOPITT), optical pa edn., 2016.

Edwards, D. P., Halvorson, C. M., and Gille, J. C.: Radiative transfer modeling for the EOS Terra satellite Measurement of Pollution in the Troposphere (MOPITT) instrument, Journal of Geophysical Research Atmospheres, 104, 16 755–16 775, https://doi.org/10.1029/1999JD900167, 1999.

Eldering, A., O'Dell, C. W., Wennberg, P. O., Crisp, D., Gunson, M. R., Viatte, C., Avis, C., Braverman, A., Castano, R., Chang, A., Chapsky, L., Cheng, C., Connor, B., Dang, L., Doran, G., Fisher, B., Frankenberg, C., Fu, D., Granat, R., Hobbs, J., Lee, R. A., Man-

drake, L., McDuffie, J., Miller, C. E., Myers, V., Natraj, V., O'Brien, D., Osterman, G. B., Oyafuso, F., Payne, V. H., Pollock, H. R., Polonsky, I., Roehl, C. M., Rosenberg, R., Schwandner, F., Smyth, M., Tang, V., Taylor, T. E., To, C., Wunch, D., and Yoshimizu, J.: The Orbiting Carbon Observatory-2: First 18 months of science data products, Atmospheric Measurement Techniques, 10, 549–563, https://doi.org/10.5194/amt-10-549-2017, 2017.

Feist, D. G., Arnold, S. G., John, N., and Geibel, M. C.: TCCON data from Ascension Island (SH), Release GGG2014R0, TCCON data archive, hosted by CaltechDATA, https://doi.org/10.14291/tccon.ggg2014.ascension01.R0/1149285, https://tccondata.org, 2014.

Fortems-Cheiney, A., Chevallier, F., Pison, I., Bousquet, P., Szopa, S., Deeter, M. N., and Clerbaux, C.: Ten years of CO emissions as seen from Measurements of Pollution in the Troposphere (MOPITT), Journal of Geophysical Research Atmospheres, 116, 1–17, https://doi.org/10.1029/2010JD014416, 2011.

Friedlingstein, P., Meinshausen, M., Arora, V. K., Jones, C. D., Anav, A., Liddicoat, S. K., and Knutti, R.: Uncertainties in CMIP5 climate projections due to carbon cycle feedbacks, Journal of Climate, 27, 511–526, https://doi.org/10.1175/JCLI-D-12-00579.1, 2014.

Friedlingstein, P., Sullivan, M. O., Jones, M. W., Andrew, R. M., and Hauck, J.: Global Carbon Budget 2020, Earth System Science Data, 2020, 3269–3340, 2020.

Giglio, L., Csiszar, I., and Justice, C. O.: Global distribution and seasonality of active fires as observed with the Terra and Aqua Moderate Resolution Imaging Spectroradiometer (MODIS) sensors, Journal of Geophysical Research: Biogeosciences, 111, 1–12, https://doi.org/10.1029/2005JG000142, 2006.

Giglio, L., Randerson, J. T., van der Werf, G. R., Kasibhatla, P. S., Collatz, G. J., Morton, D. C., and DeFries, R. S.: Assessing variability and long-term trends in burned area by merging multiple satellite fire products, Biogeosciences Discussions, 6, 11 577–11 622, https://doi.org/10.5194/bgd-6-11577-2009, 2009.

Giglio, L., Randerson, J. T., and Van Der Werf, G. R.: Analysis of daily, monthly, and annual burned area using the fourth-generation global fire emissions database (GFED4), Journal of Geophysical Research: Biogeosciences, 118, 317–328, https://doi.org/10.1002/jgrg.20042, 2013.

Gilbert, J. C. and Lemaréchal, C.: Browining1968VAD.pdf, Mathematical Programming, 45, 407–435, https://doi.org/10.1127/0941-2948/2007/0220, 1989.

Global Forest Watch: We Lost a Football Pitch of Primary Rainforest Every 6 Seconds in 2019, https://www.globalforestwatch.org/blog/data-and-research/global-tree-cover-loss-data-2019/, 2020.

Goo, T.-Y., Oh, Y.-S., and Velazco, V. A.: TCCON data from Anmeyondo (KR), Release GGG2014R0, TCCON data archive, hosted by CaltechDATA, https://doi.org/10.14291/tccon.ggg2014.anmeyondo01.R0/1149284, https://tccondata.org, 2014.

Granier, C., Bessagnet, B., Bond, T., D'Angiola, A., van der Gon, H. D., Frost, G. J., Heil, A., Kaiser, J. W., Kinne, S., Klimont, Z., Kloster, S., Lamarque, J. F., Liousse, C., Masui, T., Meleux, F., Mieville, A., Ohara, T., Raut, J. C., Riahi, K., Schultz, M. G., Smith, S. J., Thompson, A., van Aardenne, J., van der Werf, G. R., and van Vuuren, D. P.: Evolution of anthropogenic and biomass burning emissions of air pollutants at global and regional scales during the 1980-2010 period, Climatic Change, 109, 163–190, https://doi.org/10.1007/s10584-011-0154-1, 2011.

Griffith, D. W. T., Deutscher, N. M., Velazco, V. A., Wennberg, P. O., Yavin, Y., Aleks, G. K., Washenfelder, R. a., Toon, G. C., Blavier, J.-F., Murphy, C., Jones, N., Kettlewell, G., Connor, B. J., Macatangay, R., Roehl, C., Ryczek, M., Glowacki, J., Culgan, T., and Bryant, G.: TCCON data from Darwin (AU), Release GGG2014R0, TCCON data archive, hosted by CaltechDATA, https://doi.org/10.14291/tccon.ggg2014.darwin01.R0/1149290, https://tccondata.org, 2014a.

Griffith, D. W. T., Velazco, V. A., Deutscher, N. M., Murphy, C., Jones, N., Wilson, S., Macatangay, R., Kettlewell, G., Buchholz, R. R., and Riggenbach, M.: TCCON data from Wollongong (AU), Release GGG2014R0, TCCON data archive, hosted by CaltechDATA, https://doi.org/10.14291/tccon.ggg2014.wollongong01.R0/1149291, https://tccondata.org, 2014b.

Guenther, A. B., Jiang, X., Heald, C. L., Sakulyanontvittaya, T., Duhl, T., Emmons, L. K., and Wang, X.: The model of emissions of gases and aerosols from nature version 2.1 (MEGAN2.1): An extended and updated framework for modeling biogenic emissions, Geoscientific Model Development, 5, 1471–1492, https://doi.org/10.5194/gmd-5-1471-2012, 2012.

Gurney, K. R., Law, R. M., Denning, A. S., Rayner, P. J., Baker, D., Bousquet, P., Bruhwiler, L., Chen, Y. H., Ciais, P., Fan, S., Fung, I. Y., Gloor, M., Heimann, M., Higuchi, K., John, J., Maki, T., Maksyutov, S., Masarie, K., Peylin, P., Prather, M., Pak, B. C., Randerson, J., Sarmiento, J., Taguchi, S., Takahashi, T., and Yuen, C. W.: Towards robust regional estimates of annual mean CO2 sources and sinks, Nature, 415, 626–630, 2002.

Gurney, K. R., Law, R. M., Denning, A. S., Rayner, P. J., Baker, D., Bousquet, P., Bruhwiler, L., Chen, Y. H., Ciais, P., Fan, S., Fung, I. Y., Gloor, M., Heimann, M., Higuchi, K., John, J., Kowalczyk, E., Maki, T., Maksyutov, S., Peylin, P., Prather, M., Pak, B. C., Sarmiento, J., Taguchi, S., Takahashi, T., and Yuen, C. W.: TransCom 3 CO2 inversion intercomparison: 1. Annual mean control results and sensitivity to transport and prior flux information, Tellus, Series B: Chemical and Physical Meteorology, 55, 555–579, https://doi.org/10.1034/j.1600-0889.2003.00049.x, 2003.

Guyon, P., Frank, G. P., Welling, M., Chand, D., Artaxo, P., Rizzo, L., Nishioka, G., Kolle, O., Fritsch, H., Silva Dias, M. A., Gatti, L. V., Cordova, A. M., and Andreae, M. O.: Airborne measurements of trace gas and aerosol particle emissions from biomass burning in Amazonia, Atmospheric Chemistry and Physics, 5, 2989–3002, https://doi.org/10.5194/acp-5-2989-2005, 2005.

Hase, F., Blumenstock, T., Dohe, S., Groß, J., and Kiel, M.: TCCON data from Karlsruhe (DE), Release GGG2014.R1, https://doi.org/10.14291/TCCON.GGG2014.KARLSRUHE01.R1/1182416, https://data.caltech.edu/records/278, 2015.

Hooghiemstra, P. B., Krol, M. C., Meirink, J. F., Bergamaschi, P., Van Der Werf, G. R., Novelli, P. C., Aben, I., and Röckmann, T.: Optimizing global CO emission estimates using a four-dimensional variational data assimilation system and surface network observations, Atmospheric Chemistry and Physics, 11, 4705–4723, https://doi.org/10.5194/acp-11-4705-2011, 2011.

Hooghiemstra, P. B., Krol, M. C., Bergamaschi, P., De Laat, A. T. J., Van Der Werf, G. R., Novelli, P. C., Deeter, M. N., Aben, I., and Rckmann, T.: Comparing optimized CO emission estimates using MOPITT or NOAA surface network observations, Journal of Geophysical Research Atmospheres, 117, 1–23, https://doi.org/10.1029/2011JD017043, 2012.

Hooijer, A. and Vernimmen, R.: Quick Assessment and Nationwide Screening (QANS) of Peat and Lowland Resources and Action Planning for the Implementation of a National Lowland Strategy Technical Guidance for Peatland Policy Development, Ede, The Netherlands: Partners for Water Programme, 2013.

Houweling, S., Baker, D., Basu, S., Boesch, H., Butz, A., Chevallier, F., Deng, F., Dlugokencky, E. J., Feng, L., Ganshin, A., Hasekamp, O., Jones, D., Maksyutov, S., Marshall, J., Oda, T., O'Dell, C. W., Oshchepkov, S., Palmer, P. I., Peylin, P., Poussi, Z., Reum, F., Takagi, H., Yoshida, Y., and Zhuravlev, R.: An intercomparison of inversemodels for estimating sources and sinks of CO2 using GOSAT measurements, Journal of Geophysical Research, 120, 5253–5266, https://doi.org/10.1002/2014JD022962, 2015.

Huijnen, V., Williams, J., Van Weele, M., Van Noije, T., Krol, M., Dentener, F., Segers, A., Houweling, S., Peters, W., De Laat, J., Boersma, F., Bergamaschi, P., Van Velthoven, P., Le Sager, P., Eskes, H., Alkemade, F., Scheele, R., Nédélec, P., and Pätz, H. W.: The global chemistry transport model TM5: Description and evaluation of the tropospheric chemistry version 3.0, Geoscientific Model Development, 3, 445–473, https://doi.org/10.5194/gmd-3-445-2010, 2010.

Huijnen, V., Wooster, M. J., Kaiser, J. W., Gaveau, D. L., Flemming, J., Parrington, M., Inness, A., Murdiyarso, D., Main, B., and Van Weele, M.: Fire carbon emissions over maritime southeast Asia in 2015 largest since 1997, Scientific Reports, 6, 1–8, https://doi.org/10.1038/srep26886, http://dx.doi.org/10.1038/srep26886, 2016.

IPCC: Climate Change 2014 : Synthesis Report. Contribution of Working Groups I, II and III to the fifth Assessement Report of the Intergovernmental Panel on Climate Change, https://doi.org/10.1017/CBO9781107415324, 2014.

Iraci, L. T., Podolske, J., Hillyard, P. W., Roehl, C., Wennberg, P. O., Blavier, J.-F., Allen, N., Wunch, D., Osterman, G. B., and Albertson, R.: TCCON data from Edwards (US), Release GGG2014R1, TCCON data archive, hosted by CaltechDATA, https://doi.org/10.14291/tccon.ggg2014.edwards01.R1/1255068, https://tccondata.org, 2016.

Kaiser, J. W., Heil, A., Andreae, M. O., Benedetti, A., Chubarova, N., Jones, L., Morcrette, J. J., Razinger, M., Schultz, M. G., Suttie, M., and Van Der Werf, G. R.: Biomass burning emissions estimated with a global fire assimilation system based on observed fire radiative power, Biogeosciences, 9, 527–554, https://doi.org/10.5194/bg-9-527-2012, 2012.

Kawakami, S., Ohyama, H., Arai, K., Okumura, H., Taura, C., Fukamachi, T., and Sakashita, M.: TCCON data from Saga (JP), Release GGG2014R0, TCCON data archive, hosted by CaltechDATA, https://doi.org/10.14291/tccon.ggg2014.saga01.R0/1149283, https://tccondata.org, 2014.

Khatiwala, S., Primeau, F., and Hall, T.: Reconstruction of the history of anthropogenic CO2 concentrations in the ocean, Nature, 462, 346–349, https://doi.org/10.1038/nature08526, 2009.

Khatiwala, S., Tanhua, T., Mikaloff Fletcher, S., Gerber, M., Doney, S. C., Graven, H. D., Gruber, N., McKinley, G. A., Murata, A., Ríos, A. F., and Sabine, C. L.: Global ocean storage of anthropogenic carbon, Biogeosciences, 10, 2169–2191, https://doi.org/10.5194/bg-10-2169-2013, 2013.

Kiel, M., O'Dell, C. W., Fisher, B., Eldering, A., Nassar, R., MacDonald, C. G., and Wennberg, P. O.: How bias correction goes wrong: Measurement of XCO2 affected by erroneous surface pressure estimates, Atmospheric Measurement Techniques Discussions, pp. 1–38, https://doi.org/10.5194/amt-2018-353, 2019.

Kivi, R., Heikkinen, P., and Kyrö, E.: TCCON data from Sodankyla (FI), Release GGG2014R0, TCCON data archive, hosted by CaltechDATA, https://doi.org/10.14291/tccon.ggg2014.sodankyla01.R0/1149280, https://tccondata.org, 2014.

Konovalov, I. B., Berezin, E. V., Ciais, P., Broquet, G., Beekmann, M., Hadji-Lazaro, J., Clerbaux, C., Andreae, M. O., Kaiser, J. W., and Schulze, E. D.: Constraining CO2emissions from open biomass burning by satellite observations of co-emitted species: A method and its application to wildfires in Siberia, Atmospheric Chemistry and Physics, 14, 10 383–10 410, https://doi.org/10.5194/acp-14-10383-2014, 2014.

Krol, M., Houweling, S., Bregman, B., van den Broek, M., Segers, A., van Velthoven, P., Peters, W., Dentener, F., and Bergamaschi, P.: The two-way nested global chemistry-transport zoom model TM5: algorithm and applications, Atmospheric Chemistry and Physics Discussions, 4, 3975–4018, https://doi.org/10.5194/acpd-4-3975-2004, 2005.

Kulawik, S., Wunch, D., O'Dell, C., Frankenberg, C., Reuter, M., Oda, T., Chevallier, F., Sherlock, V., Buchwitz, M., Osterman, G., Miller, C. E., Wennberg, P. O., Griffith, D., Morino, I., Dubey, M. K., Deutscher, N. M., Notholt, J., Hase, F., Warneke, T., Sussmann, R., Robinson, J., Strong, K., Schneider, M., De Mazière, M., Shiomi, K., Feist, D. G., Iraci, L. T., and Wolf, J.: Consistent evaluation of ACOS-GOSAT, BESD-SCIAMACHY, CarbonTracker, and MACC through comparisons to TCCON, Atmospheric Measurement Techniques, 9, 683–709, https://doi.org/10.5194/amt-9-683-2016, 2016.

Kuze, A., Suto, H., Nakajima, M., and Hamazaki, T.: Initial Onboard Performance of TANSO-FTS on GOSAT, in: Advances in Imaging, p. FTuC2, Optical Society of America, https://doi.org/10.1364/FTS.2009.FTuC2, http://www.osapublishing.org/abstract.cfm?URI=FTS-2009-FTuC2, 2009.

Landgraf, J., Aan De Brugh, J., Scheepmaker, R., Borsdorff, T., Hu, H., Houweling, S., Butz, A., Aben, I., and Hasekamp, O.: Carbon monoxide total column retrievals from TROPOMI shortwave infrared measurements, Atmospheric Measurement Techniques, 9, 4955–4975, https://doi.org/10.5194/amt-9-4955-2016, 2016.

Lauvaux, T., Schuh, A. E., Bocquet, M., Wu, L., Richardson, S., Miles, N., and Davis, K. J.: Network design for mesoscale inversions of CO 2 sources and sinks, Tellus, Series B: Chemical and Physical Meteorology, 64, 1–12, https://doi.org/10.3402/tellusb.v64i0.17980, 2012a.

Lauvaux, T., Schuh, A. E., Uliasz, M., Richardson, S., Miles, N., Andrews, A. E., Sweeney, C., Diaz, L. I., Martins, D., Shepson, P. B., and Davis, K. J.: Constraining the CO2 budget of the corn belt: Exploring uncertainties from the assumptions in a mesoscale inverse system, Atmospheric Chemistry and Physics, 12, 337–354, https://doi.org/10.5194/acp-12-337-2012, 2012b.

Le Quéré, C., Raupach, M. R., Canadell, J. G., Marland, G., Bopp, L., Ciais, P., Conway, T. J., Doney, S. C., Feely, R. A., Foster, P., Friedlingstein, P., Gurney, K., Houghton, R. A., House, J. I., Huntingford, C., Levy, P. E., Lomas, M. R., Majkut, J., Metzl, N., Ometto, J. P., Peters, G. P., Prentice, I. C., Randerson, J. T., Running, S. W., Sarmiento, J. L., Schuster, U., Sitch, S., Takahashi, T., Viovy, N., Van Der Werf, G. R., and Woodward, F. I.: Trends in the sources and sinks of carbon dioxide, Nature Geoscience, 2, 831–836, https://doi.org/10.1038/ngeo689, 2009.

Le Quéré, C., Andrew, R. M., Friedlingstein, P., Sitch, S., Pongratz, J., Manning, A. C., Korsbakken, J. I., Peters, G. P., Canadell, J. G., Jackson, R. B., Boden, T. A., Tans, P. P., Andrews, O. D., Arora, V. K., Bakker, D. C. E., Barbero, L., Becker, M., Betts, R. A., Bopp, L., Chevallier, F., Chini, L. P., Ciais, P., Cosca, C. E., Cross, J., Currie, K., Gasser, T., Harris, I., Hauck, J., Haverd, V., Houghton, R. A., Hunt, C. W., Hurtt, G., Ilyina, T., Jain, A. K., Kato, E., Kautz, M., Keeling, R. F., Klein Goldewijk, K., Körtzinger, A., Landschützer, P., Lefèvre, N., Lenton, A., Lienert, S., Lima, I., Lombardozzi, D., Metzl, N., Millero, F., Monteiro, P. M. S., Munro, D. R., Nabel, J. E. M. S., Nakaoka, S.-i., Nojiri, Y., Padín, X. A., Peregon, A., Pfeil, B., Pierrot, D., Poulter, B., Rehder, G., Reimer, J., Rödenbeck, C., Schwinger, J., Séférian, R., Skjelvan, I., Stocker, B. D., Tian, H., Tilbrook, B., van der Laan-Luijkx, I. T., van der Werf, G. R., van Heuven, S., Viovy, N., Vuichard, N., Walker, A. P., Watson, A. J., Wiltshire, A. J., Zaehle, S., and Zhu, D.: Global Carbon Budget 2018 (pre-print), Earth System Science Data Discussions, pre print, 1–54, https://www.earth-syst-sci-data.net/10/2141/2018/essd-10-2141-2018.pdf, 2018.

Liu, J., Rodriguez, J. M., Steenrod, S. D., Douglass, A. R., Logan, J. A., Olsen, M. A., Wargan, K., and Ziemke, J. R.: Causes of interannual variability over the southern hemispheric tropospheric ozone maximum, Atmospheric Chemistry and Physics, 17, 3279–3299, https://doi.org/10.5194/acp-17-3279-2017, 2017a.

Liu, J. C., Wilson, A., Mickley, L. J., Dominici, F., Ebisu, K., Wang, Y., Sulprizio, M. P., Peng, R. D., Yue, X., Son, J. Y., Anderson, G. B., and Bell, M. L.: Wildfire-specific fine particulate matter and risk of hospital admissions in urban and rural counties, Epidemiology, 28, 77–85, https://doi.org/10.1097/EDE.0000000000000556, 2017b.

Liu, T., Mickley, L. J., Marlier, M. E., DeFries, R. S., Khan, M. F., Latif, M. T., and Karambelas, A.: Diagnosing spatial biases and uncertainties in global fire emissions inventories: Indonesia as regional case study, Remote Sensing of Environment, 237, 111 557, https://doi.org/10.1016/j.rse.2019.111557, https://doi.org/10.1016/j.rse.2019.111557, 2020.

Logan, J. A., Prather, M. J., Wofsy, S. C., and Mcelroy, M. B.: Tropospheric chemistry: A global perspective, Journal of Geophysical Research, 86, 7210–7254, 1981.

Lohberger, S., Stangel, M., Atwood, E., and Siegert, F.: Spatial evaluation of Indonesia's 2015 fire affected area and estimated carbon emissions using Sentinel-1, Global Change Biology, 24, 644–654, https://doi.org/doi:10. 1111/gcb.13841, 2017.

Masarie, K. A., Peters, W., Jacobson, A. R., and Tans, P. P.: ObsPack: A framework for the preparation, delivery, and attribution of atmospheric greenhouse gas measurements, Earth System Science Data, 6, 375–384, https://doi.org/10.5194/essd-6-375-2014, 2014.

Meirink, J. F., Bergamaschi, P., Frankenberg, C., D'Amelio, M. T., Dlugokencky, E. J., Gatti, L. V., Houweling, S., Miller, J. B., Röckmann, T., Villani, M. G., and Krol, M. C.: Four-dimensional variational data assimilation for inverse modeling of atmospheric methane emissions: Analysis of SCIAMACHY observations, Journal of Geophysical Research Atmospheres, 113, 1–20, https://doi.org/10.1029/2007JD009740, 2008.

Moore, B., Crowell, S. M., Rayner, P. J., Kumer, J., O'Dell, C. W., O'Brien, D., Utembe, S., Polonsky, I., Schimel, D., and Lemen, J.: The Potential of the Geostationary Carbon Cycle Observatory (GeoCarb) to provide multi-scale constraints on the carbon cycle in the Americas, Frontiers in Environmental Science, 6, 1–13, https://doi.org/10.3389/fenvs.2018.00109, 2018.

Morino, I., Matsuzaki, T., and Horikawa, M.: TCCON data from Tsukuba (JP), 125HR, Release GGG2014.R2, https://doi.org/10.14291/TCCON.GGG2014.TSUKUBA02.R2, https://data.caltech.edu/records/958, 2018a.

Morino, I., Yokozeki, N., Matsuzaki, T., and Horikawa, M.: TCCON data from Rikubetsu (JP), Release GGG2014.R2, https://doi.org/10.14291/TCCON.GGG2014.RIKUBETSU01.R2, https://data.caltech.edu/records/957, 2018b.

Nara, H., Tanimoto, H., Tohjima, Y., Mukai, H., Nojiri, Y., and Machida, T.: Emission factors of CO2, CO and CH4 from Sumatran peatland fires in 2013 based on shipboard measurements, Tellus B: Chemical and Physical Meteorology, 69, 1399 047, https://doi.org/10.1080/16000889.2017.1399047, https://doi.org/10.1080/16000889.2017.1399047, 2017.

Nassar, R., Napier-Linton, L., Gurney, K. R., Andres, R. J., Oda, T., Vogel, F. R., and Deng, F.: Improving the temporal and spatial distribution of co2 emissions from global fossil fuel emission data sets, Journal of Geophysical Research Atmospheres, 118, 917–933, https://doi.org/10.1029/2012JD018196, 2013.

Nechita-Banda, N., Krol, M., van der Werf, G. R., Kaiser, J. W., Pandey, S., Huijnen, V., Clerbaux, C., Coheur, P., Deeter, M. N., and Röckmann, T.: Monitoring emissions from the 2015 Indonesian fires using CO satellite data, Philosophical Transactions of the Royal Society B: Biological Sciences, 373, 20170 307, https://doi.org/10.1098/rstb.2017.0307, https://www.deltares.nl/app/uploads/2015/03/QANS-Peat-mapping-report-final-with-cover.pdf, 2018.

Nechita-banda, N., Krol, M., Werf, G. R. V. D., Kaiser, J. W., Pandey, S., Huijnen, V., Clerbaux, C., Coheur, P., Deeter, M. N., and Ro, T.: Monitoring emissions from the 2015 Indonesian fires using CO satellite data, Philosophical Transactions of the Royal Society B, 373, https://doi.org/10.1098/rstb.2017.0307, 2018.

NOAA Carbon Cycle Group ObsPack Team: INPE atmospheric carbon dioxide data for the period 2015-2017; {obspack_co2_1_INPE_RESTRICTED_v2.0_2018-11-13}, https://doi.org/10.25925/20181030, http://www.esrl.noaa.gov/gmd/ccgg/obspack/data.php?id=obspack{_}co2{_}1{_}INPE{_}RESTRICTED{_}v2.0{_}2018-11-13, 2018.

NOAA Carbon Cycle Group ObsPack Team: Multi-laboratory compilation of atmospheric carbon dioxide data for the years 2018-2019; {obspack_co2_1_NRT_v5.0_2019-08-13}, https://doi.org/10.25925/20190813, http://www.esrl.noaa.gov/gmd/ccgg/obspack/data.php?id=obspack{_}co2{_}1{_}NRT{_}v5.0{_}2019-08-13, 2019.

Notholt, J., Petri, C., Warneke, T., Deutscher, N. M., Buschmann, M., Weinzierl, C., Macatangay, R., and Grupe, P.: TCCON data from Bremen (DE), Release GGG2014R0, TCCON data archive, hosted by CaltechDATA, https://doi.org/10.14291/tccon.ggg2014.bremen01.R0/1149275, https://tccondata.org, 2014a.

Notholt, J., Warneke, T., Petri, C., Deutscher, N. M., Weinzierl, C., Palm, M., and Buschmann, M.: TCCON data from Ny Ålesund, Spitsbergen (NO), Release GGG2014.R0, https://doi.org/10.14291/TCCON.GGG2014.NYALESUND01.R0/1149278, https://data.caltech.edu/records/301, 2014b.

Oda, T. and Maksyutov, S.: A very high-resolution (1km×1 km) global fossil fuel CO 2 emission inventory derived using a point source database and satellite observations of nighttime lights, Atmospheric Chemistry and Physics, 11, 543–556, https://doi.org/10.5194/acp-11-543-2011, 2011.

O'Dell, C. W., Connor, B., Bösch, H., O'Brien, D., Frankenberg, C., Castano, R., Christi, M., Eldering, D., Fisher, B., Gunson, M., McDuffie, J., Miller, C. E., Natraj, V., Oyafuso, F., Polonsky, I., Smyth, M., Taylor, T., Toon, G. C., Wennberg, P. O., and Wunch, D.: The ACOS CO2 retrieval algorithm-Part 1: Description and validation against synthetic observations, Atmospheric Measurement Techniques, 5, 99–121, https://doi.org/10.5194/amt-5-99-2012, 2012.

O'Dell, C. W., Eldering, A., Wennberg, P. O., Crisp, D., Gunson, M. R., Fisher, B., Frankenberg, C., Kiel, M., Lindqvist, H., Mandrake, L., Merrelli, A., Natraj, V., Nelson, R. R., Osterman, G. B., Payne, V. H., Taylor, T. E., Wunch, D., Drouin, B. J., Oyafuso, F., Chang, A., McDuffie, J., Smyth, M., Baker, D. F., Basu, S., Chevallier, F., Crowell, S. M., Feng, L., Palmer, D. P. I., Dubey, M., García, O. E., Griffith, D. W., Hase, F., Iraci, L. T., Kivi, R., Morino, I., Notholt, J., Ohyama, H., Petri, C., Roehl, C. M., Sha, M. K., Strong, K., Sussmann, R., Te, Y., Uchino, O., and Velazco, V. A.: Improved retrievals of carbon dioxide from Orbiting Carbon Observatory-2 with the version 8 ACOS algorithm, Atmospheric Measurement Techniques, 11, 6539–6576, https://doi.org/10.5194/amt-11-6539-2018, 2018.

Ott, L.: GEOS-Carb CASA-GFED 3-hourly Ecosystem Exchange Fluxes 0.5 degree x 0.625 degree V3, Greenbelt, MD, USA, Goddard Earth Sciences Data and Information Services Center (GES DISC), https://doi.org/10.5067/VQPRALE26L20, 2020.

Palmer, P. I., Feng, L., Baker, D., Chevallier, F., Bösch, H., and Somkuti, P.: Net carbon emissions from African biosphere dominate pan-tropical atmospheric CO2 signal, Nature Communications, 10, 1–10, https://doi.org/10.1038/s41467-019-11097-w, http://dx.doi.org/10.1038/s41467-019-11097-w, 2019.

Patra, P. K., Crisp, D., Kaiser, J. W., Wunch, D., Saeki, T., Ichii, K., Sekiya, T., Wennberg, P. O., Feist, D. G., Pollard, D. F., Griffith, D. W., Velazco, V. A., De Maziere, M., Sha, M. K., Roehl, C., Chatterjee, A., and Ishijima, K.: The Orbiting Carbon Observatory (OCO-2) tracks 2-3 peta-gram increase in carbon release to the atmosphere during the 2014-2016 El Niño, Scientific Reports, 7, 1–12, https://doi.org/10.1038/s41598-017-13459-0, 2017.

Pechony, O., Shindell, D. T., and Faluvegi, G.: Direct top-down estimates of biomass burning CO emissions using TES and MOPITT versus bottom-up GFED inventory, Journal of Geophysical Research Atmospheres, 118, 8054–8066, https://doi.org/10.1002/jgrd.50624, 2013.

Peiro, H., Crowell, S., Schuh, A., Baker, D. F., O'Dell, C., Jacobson, A. R., Chevallier, F., Liu, J., Eldering, A., Crisp, D., Deng, F., Weir, B., Basu, S., Johnson, M. S., Philip, S., and Baker, I.: Four years of global carbon cycle observed from the Orbiting Carbon Observatory 2 (OCO-2) version 9 and in situ data and comparison to OCO-2 version 7, Atmospheric Chemistry and Physics, 22, 1097–1130, https://doi.org/10.5194/acp-22-1097-2022, https://acp.copernicus.org/articles/22/1097/2022/, 2022.

Peters, W., Jacobson, A. R., Sweeney, C., Andrews, A. E., Conway, T. J., Masarie, K., Miller, J. B., Bruhwiler, L. M., Pétron, G., Hirsch, A. I., Worthy, D. E., Van Der Werf, G. R., Randerson, J. T., Wennberg, P. O., Krol, M. C., and Tans, P. P.: An atmospheric perspective on North American carbon dioxide exchange: CarbonTracker, Proceedings of the National Academy of Sciences of the United States of America, 104, 18 925–18 930, https://doi.org/10.1073/pnas.0708986104, 2007.

Pétron, G., Granier, C., Khattatov, B., Lamarque, J. F., Yudin, V., Müller, J. F., and Gille, J.: Inverse modeling of carbon monoxide surface emissions using Climate Monitoring and Diagnostics Laboratory network observations, Journal of Geophysical Research Atmospheres, 107, 1–23, https://doi.org/10.1029/2001JD001305, 2002.

Peylin, P., Law, R. M., Gurney, K. R., Chevallier, F., Jacobson, A. R., Maki, T., Niwa, Y., Patra, P. K., Peters, W., Rayner, P. J., Rödenbeck, C., Van Der Laan-Luijkx, I. T., and Zhang, X.: Global atmospheric carbon budget: Results from an ensemble of atmospheric CO2 inversions, Biogeosciences, 10, 6699–6720, https://doi.org/10.5194/bg-10-6699-2013, 2013.

Pfister, G. G., Emmons, L. K., Hess, P. G., Lamarque, J. F., Orlando, J. J., Walters, S., Guenther, A., Palmer, P. I., and Lawrence, P. J.: Contribution of isoprene to chemical budgets: A model tracer study with the NCAR CTM MOZART-4, Journal of Geophysical Research Atmospheres, 113, https://doi.org/10.1029/2007JD008948, 2008.

Philip, S., Johnson, M. S., Potter, C., Genovesse, V., Baker, D. F., Haynes, K. D., Henze, D. K., Liu, J., and Poulter, B.: Prior biosphere model impact on global terrestrial CO2 fluxes estimated from OCO-2 retrievals, Atmospheric Chemistry and Physics, 19, 13 267–13 287, https://doi.org/10.5194/acp-19-13267-2019, 2019.

Potosnak, M. J., Wofsy, C., Denning, A. S., Munger, J. W., and Barnes, D. H.: Influence of biotic exchange and combustion sources on atmospheric CO2 concentrations in New England from observations at a forest flux tower, Journal of Geophysical Research, 104, 9561–9569, 1999.

Quéré, C. L., Andrew, R. M., Friedlingstein, P., Sitch, S., and Hauck, J.: Global Carbon Budget 2018, Earth System Science Data (Online), 10, 2141–2194, 2018.

Quilcaille, Y., Gasser, T., Ciais, P., Lecocq, F., Janssens-Maenhout, G., and Mohr, S.: Uncertainty in projected climate change arising from uncertain fossil-fuel emission factors, Environmental Research Letters, 13, https://doi.org/10.1088/1748-9326/aab304, 2018.

Ramo, R., Roteta, E., Bistinas, I., van Wees, D., Bastarrika, A., Chuvieco, E., and van der Werf, G. R.: African burned area and fire carbon emissions are strongly impacted by small fires undetected by coarse resolution satellite data, Proceedings of the National Academy of Sciences of the United States of America, 118, 1–7, https://doi.org/10.1073/pnas.2011160118, 2021.

Randerson, J. T., Chen, Y., Van Der Werf, G. R., Rogers, B. M., and Morton, D. C.: Global burned area and biomass burning emissions from small fires, Journal of Geophysical Research G: Biogeosciences, 117, https://doi.org/10.1029/2012JG002128, 2012.

Reuter, M., Buchwitz, M., Hilker, M., Heymann, J., Schneising, O., and Pillai, D.: Satellite-inferred European carbon sink larger than expected, Atmospheric Chemistry and Physics Discussions, 14, 21 829–21 863, https://doi.org/10.5194/acpd-14-21829-2014, 2014.

Reuter, M., Buchwitz, M., Hilker, M., Heymann, J., Bovensmann, H., Burr Ows, J. P., Houweling, S., Liu, Y. Y., Nassar, R., Chevallier, F., Ciais, P., Marshall, J., and Reichstein, M.: How much CO2 is taken up by the European terrestrial biosphere?, Bulletin of the American Meteorological Society, 98, 665–671, https://doi.org/10.1175/BAMS-D-15-00310.1, 2017.

Rodgers, C.: Inverse Methods for Atmospheric Sounding - Theory and Practice, World Scientific Publishing, 2, https://doi.org/10.1142/9789812813718, 2000.

Rothman, L. S., Gordon, I. E., Babikov, Y., Barbe, A., Chris Benner, D., Bernath, P. F., Birk, M., Bizzocchi, L., Boudon, V., Brown, L. R., Campargue, A., Chance, K., Cohen, E. A., Coudert, L. H., Devi, V. M., Drouin, B. J., Fayt, A., Flaud, J. M., Gamache, R. R., Harrison, J. J., Hartmann, J. M., Hill, C., Hodges, J. T., Jacquemart, D., Jolly, A., Lamouroux, J., Le Roy, R. J., Li, G., Long, D. A., Lyulin, O. M., Mackie, C. J., Massie, S. T., Mikhailenko, S., Müller, H. S., Naumenko, O. V., Nikitin, A. V., Orphal, J., Perevalov, V., Perrin, A., Polovtseva, E. R., Richard, C., Smith, M. A., Starikova, E., Sung, K., Tashkun, S., Tennyson, J., Toon, G. C., Tyuterev, V. G., and Wagner, G.: The HITRAN2012 molecular spectroscopic database, Journal of Quantitative Spectroscopy and Radiative Transfer, 130, 4–50, https://doi.org/10.1016/j.jqsrt.2013.07.002, 2013.

Schuh, A. E., Jacobson, A. R., Basu, S., Weir, B., Baker, D., Bowman, K., Chevallier, F., Crowell, S., Davis, K. J., Deng, F., Denning, S., Feng, L., Jones, D., Liu, J., and Palmer, P. I.: Quantifying the Impact of Atmospheric Transport Uncertainty on CO2 Surface Flux Estimates, Global Biogeochemical Cycles, 33, 484–500, https://doi.org/10.1029/2018GB006086, 2019.

Sherlock, V., Connor, B. J., Robinson, J., Shiona, H., Smale, D., and Pollard, D.: TCCON data from Lauder (NZ), 125HR, Release GGG2014.R0, TCCON data archive, hosted by CaltechDATA, https://doi.org/10.14291/TCCON.GGG2014.LAUDER02.R0/1149298, 2014.

Shi, Y., Matsunaga, T., Saito, M., Yamaguchi, Y., and Chen, X.: Comparison of global inventories of CO<inf>2</inf> emissions from biomass burning during 2002-2011 derived from multiple satellite products, Environmental Pollution, 206, 479–487, https://doi.org/10.1016/j.envpol.2015.08.009, http://dx.doi.org/10.1016/j.envpol.2015.08.009, 2015.

Sofiev, M., Vankevich, R., Ermakova, T., and Hakkarainen, J.: Global mapping of maximum emission heights and resulting vertical profiles of wildfire emissions, Atmospheric Chemistry and Physics, 13, 7039–7052, https://doi.org/10.5194/acp-13-7039-2013, 2013.

Spivakovsky, C. M., Logan, J. A., Montzka, S. A., Balkanski, Y. J., Foreman-Fowler, M., Jones, D. B., Horowitz, L. W., Fusco, A. C., Brenninkmeijer, C. A., Prather, M. J., Wofsy, S. C., and McElroy, M. B.: Three-dimensional climatological distribution of tropospheric OH: Update and evaluation, Journal of Geophysical Research Atmospheres, 105, 8931–8980, https://doi.org/10.1029/1999JD901006, 2000.

Strong, K., Roche, S., Franklin, J. E., Mendonca, J., Lutsch, E., Weaver, D., Fogal, P. F., Drummond, J. R., Batchelor, R., and Lindenmaier, R.: TCCON data from Eureka (CA), Release GGG2014.R3, https://doi.org/10.14291/TCCON.GGG2014.EUREKA01.R3, https://data.caltech.edu/records/1171, 2019.

Sussmann, R. and Rettinger, M.: TCCON data from Garmisch (DE), Release GGG2014.R2, https://doi.org/10.14291/TCCON.GGG2014.GARMISCH01.R2, https://data.caltech.edu/records/956, 2018.

Takahashi, T., Sutherland, S. C., Wanninkhof, R., Sweeney, C., Feely, R. A., Chipman, D. W., Hales, B., Friederich, G., Chavez, F., Sabine, C., Watson, A., Bakker, D. C., Schuster, U., Metzl, N., Yoshikawa-Inoue, H., Ishii, M., Midorikawa, T., Nojiri, Y., Körtzinger, A., Steinhoff, T., Hoppema, M., Olafsson, J., Arnarson, T. S., Tilbrook, B., Johannessen, T., Olsen, A., Bellerby, R., Wong, C. S., Delille, B., Bates, N. R., and de Baar, H. J.: Corrigendum to "Climatological mean and decadal change in surface ocean pCO 2 , and net sea-air CO 2 flux over the global oceans", https://doi.org/10.1016/j.dsr.2009.07.007, 2009.

Té, Y., Jeseck, P., and Janssen, C.: TCCON data from Paris (FR), Release GGG2014.R0, https://doi.org/10.14291/TCCON.GGG2014.PARIS01.R0/1149279, https://data.caltech.edu/records/284, 2014.

Tohjima, Y., Mukai, H., Machida, T., Nojiri, Y., and Gloor, M.: First measurements of the latitudinal atmospheric O2 and CO2 distributions across the western Pacific, Geophysical Research Letters, 32, https://doi.org/https://doi.org/10.1029/2005GL023311, https://agupubs.onlinelibrary.wiley.com/doi/abs/10.1029/2005GL023311, 2005.

Tsigaridis, K., Daskalakis, N., Kanakidou, M., Adams, P. J., Artaxo, P., Bahadur, R., Balkanski, Y., Bauer, S. E., Bellouin, N., Benedetti, A., Bergman, T., Berntsen, T. K., Beukes, J. P., Bian, H., Carslaw, K. S., Chin, M., Curci, G., Diehl, T., Easter, R. C., Ghan, S. J., Gong, S. L., Hodzic, A., Hoyle, C. R., Iversen, T., Jathar, S., Jimenez, J. L., Kaiser, J. W., Kirkeväg, A., Koch, D., Kokkola, H., H Lee, Y., Lin, G., Liu, X., Luo, G., Ma, X., Mann, G. W., Mihalopoulos, N., Morcrette, J. J., Müller, J. F., Myhre, G., Myriokefalitakis, S., Ng, N. L., O'donnell, D., Penner, J. E., Pozzoli, L., Pringle, K. J., Russell, L. M., Schulz, M., Sciare, J., Seland, Shindell, D. T., Sillman, S., Skeie, R. B., Spracklen, D., Stavrakou, T., Steenrod, S. D., Takemura, T., Tiitta, P., Tilmes, S., Tost, H., Van Noije, T., Van Zyl, P. G., Von Salzen, K., Yu, F., Wang, Z., Wang, Z., Zaveri, R. A., Zhang, H., Zhang, K., Zhang, Q., and Zhang, X.: The AeroCom evaluation and intercomparison of organic aerosol in global models, Atmospheric Chemistry and Physics, 14, 10 845–10 895, https://doi.org/10.5194/acp-14-10845-2014, 2014.

Turnbull, J. C., Miller, J. B., Lehman, S. J., Tans, P. P., Sparks, R. J., and Southon, J.: Comparison of 14CO2, CO, and SF6 as tracers for recently added fossil fuel CO2 in the atmosphere and implications for biological CO2 exchange, Geophysical Research Letters, 33, 2–6, https://doi.org/10.1029/2005GL024213, 2006.

Turquety, S., Clerbaux, C., Hauglustaine, D. A., Clough, S. A., Schlu, P., and Me, G.: Operational trace gas retrieval algorithm for the Infrared Atmospheric Sounding Interferometer, Journal of Geophysical Research, 109, 1–19, https://doi.org/10.1029/2004JD004821, 2004.

van der Laan-Luijkx, I. T., Krol, M. C., Gatti, L. V., Domingues, L. G., Correia, C. S. C., Miller, J. B., Gloor, M., Leeuwen, T. T., Kaiser, J. W., Wiedinmyer, C., Basu, S., Clerbaux, C., and Peters, W.: Response of the Amazon carbon balance to the 2010 drought derived with CarbonTracker South America, Global Biogeochemical Cycles, pp. 1092–1108, https://doi.org/10.1002/2014GB005082.Received, 2015.

van der Werf, G. R., Randerson, J. T., Collatz, G. J., Giglio, L., Kasibhatla, P. S., Arellano Jr, A. F., Olsen, S. C., and Kasischke, E. S.: Continental -scale partitioning of fire emissions during 1997 to 2001 El Nino / La Nina Period, Science, 73, 73–76, 2004.

van der Werf, G. R., Randerson, J. T., Giglio, L., Collatz, G. J., Mu, M., Kasibhatla, P. S., Morton, D. C., Defries, R. S., Jin, Y., and Van Leeuwen, T. T.: Global fire emissions and the contribution of deforestation, savanna, forest, agricultural, and peat fires (1997-2009), Atmospheric Chemistry and Physics, 10, 11 707–11 735, https://doi.org/10.5194/acp-10-11707-2010, 2010.

van der Werf, G. R., Randerson, J. T., Giglio, L., Van Leeuwen, T. T., Chen, Y., Rogers, B. M., Mu, M., Van Marle, M. J., Morton, D. C., Collatz, G. J., Yokelson, R. J., and Kasibhatla, P. S.: Global fire emissions estimates during 1997-2016, Earth System Science Data, 9, 697–720, https://doi.org/10.5194/essd-9-697-2017, 2017.

Van Leeuwen, T. T., Peters, W., Krol, M. C., and Van Der Werf, G. R.: Dynamic biomass burning emission factors and their impact on atmospheric CO mixing ratios, Journal of Geophysical Research Atmospheres, 118, 6797–6815, https://doi.org/10.1002/jgrd.50478, 2013.

Venevsky, S., Le Page, Y., Pereira, J. M., and Wu, C.: Analysis fire patterns and drivers with a global SEVER-FIRE v1.0 model incorporated into dynamic global vegetation model and satellite and on-ground observations, Geoscientific Model Development, 12, 89–110, https://doi.org/10.5194/gmd-12-89-2019, 2019.

Vermote, E., Ellicott, E., Dubovik, O., Lapyonok, T., Chin, M., Giglio, L., and Roberts, G. J.: An approach to estimate global biomass burning emissions of organic and black carbon from MODIS fire radiative power, Journal of Geophysical Research Atmospheres, 114, 1–22, https://doi.org/10.1029/2008JD011188, 2009.

Wang, J. S., Kawa, S. R., Collatz, G. J., Sasakawa, M., Gatti, L. V., Machida, T., Liu, Y., and Manyin, M. E.: A Global Synthesis Inversion Analysis of Recent Variability in CO2 Fluxes Using GOSAT and In Situ Observations, Atmospheric Chemistry and Physics Discussions, 18, 11 097–11 124, https://doi.org/10.5194/acp-18-11097-2018, 2018.

Wang, Y., Munger, J. W., Xu, S., McElroy, M. B., Hao, J., Nielsen, C. P., and Ma, H.: CO2 and its correlation with CO at a rural site near Beijing: Implications for combustion efficiency in China, Atmospheric Chemistry and Physics, 10, 8881–8897, https://doi.org/10.5194/acp-10-8881-2010, 2010.

Warneke, T., Messerschmidt, J., Notholt, J., Weinzierl, C., Deutscher, N. M., Petri, C., and Grupe, P.: TCCON data from Orléans (FR), Release GGG2014.R1, https://doi.org/10.14291/TCCON.GGG2014.ORLEANS01.R1, https://data.caltech.edu/records/1301, 2019.

Wennberg, P. O., Wunch, D., Roehl, C., Blavier, J.-F., Toon, G. C., and Allen, N.: TCCON data from Caltech (US), Release GGG2014R1, TCCON data archive, hosted by CaltechDATA, https://doi.org/10.14291/tccon.ggg2014.pasadena01.R1/1182415, https://tccondata.org, 2014.

Wennberg, P. O., Wunch, D., Roehl, C., Blavier, J.-F., Toon, G. C., Allen, N., Dowell, P., Teske, K., Martin, C., and Martin., J.: TCCON data from Lamont (US), Release GGG2014R1, TCCON data archive, hosted by CaltechDATA, https://doi.org/10.14291/tccon.ggg2014.lamont01.R1/1255070, https://tccondata.org, 2016.

Wennberg, P. O., Roehl, C. M., Wunch, D., Toon, G. C., Blavier, J.-F., Washenfelder, R., Keppel-Aleks, G., Allen, N. T., and Ayers, J.: TCCON data from Park Falls (US), Release GGG2014.R1, https://doi.org/10.14291/TCCON.GGG2014.PARKFALLS01.R1, https://data.caltech.edu/records/295, 2017.

Wiedinmyer, C. and Neff, J. C.: Estimates of CO2 from fires in the United States: Implications for carbon management, Carbon Balance and Management, 2, 1–12, https://doi.org/10.1186/1750-0680-2-10, 2007.

Wiedinmyer, C., Akagi, S. K., Yokelson, R. J., Emmons, L. K., Al-Saadi, J. A., Orlando, J. J., and Soja, A. J.: The Fire INventory from NCAR (FINN): A high resolution global model to estimate the emissions from open burning, Geoscientific Model Development, 4, 625–641, https://doi.org/10.5194/gmd-4-625-2011, 2011.

Worden, H. M., Deeter, M. N., Edwards, D. P., Gille, J. C., Drummond, J. R., and Nédélec, P.: Observations of near-surface carbon monoxide from space using MOPITT multispectral retrievals, Journal of Geophysical Research Atmospheres, 115, 1–12, https://doi.org/10.1029/2010JD014242, 2010.

Wunch, D., Toon, G. C., Wennberg, P. O., Wofsy, S. C., Stephens, B. B., Fischer, M. L., Uchino, O., Abshire, J. B., Bernath, P., Biraud, S. C., Blavier, J. F., Boone, C., Bowman, K. P., Browell, E. V., Campos, T., Connor, B. J., Daube, B. C., Deutscher, N. M., Diao, M., Elkins, J. W., Gerbig, C., Gottlieb, E., Griffith, D. W., Hurst, D. F., Jiménez, R., Keppel-Aleks, G., Kort, E. A., MacAtangay, R., MacHida, T., Matsueda, H., Moore, F., Morino, I., Park, S., Robinson, J., Roehl, C. M., Sawa, Y., Sherlock, V., Sweeney, C., Tanaka, T., and Zondlo, M. A.: Calibration of the total carbon column observing network using aircraft profile data, Atmospheric Measurement Techniques, 3, 1351–1362, https://doi.org/10.5194/amt-3-1351-2010, 2010.

Wunch, D., Toon, G. C., Blavier, J. F. L., Washenfelder, R. A., Notholt, J., Connor, B. J., Griffith, D. W., Sherlock, V., and Wennberg, P. O.: The total carbon column observing network, Philosophical Transactions of the Royal Society A: Mathematical, Physical and Engineering Sciences, 369, 2087–2112, https://doi.org/10.1098/rsta.2010.0240, 2011.

Wunch, D., Wennberg, P. O., Osterman, G., Fisher, B., Naylor, B., Roehl, M. C., O'Dell, C., Mandrake, L., Viatte, C., Kiel, M., Griffith, D. W., Deutscher, N. M., Velazco, V. A., Notholt, J., Warneke, T., Petri, C., De Maziere, M., Sha, M. K., Sussmann, R., Rettinger, M., Pollard, D., Robinson, J., Morino, I., Uchino, O., Hase, F., Blumenstock, T., Feist, D. G., Arnold, S. G., Strong, K., Mendonca, J., Kivi, R., Heikkinen, P., Iraci, L., Podolske, J., Hillyard, P., Kawakami, S., Dubey, M. K., Parker, H. A., Sepulveda, E., García, O. E., Te, Y., Jeseck, P., Gunson, M. R., Crisp, D., and Eldering, A.: Comparisons of the Orbiting Carbon Observatory-2 (OCO-2) XCO2 measurements with TCCON, Atmospheric Measurement Techniques, 10, 2209–2238, https://doi.org/10.5194/amt-10-2209-2017, 2017.

Yarwood, G., Whitten, G., and Rao, S.: Updates to the Carbon Bond 4 photochemical mechanism, Environ. Int. Corp, http://www.ladco.org/reports/rpo/modeling/camx{_}cb4.pdf, 2005.

Yin, Y., Chevallier, F., Ciais, P., Broquet, G., Fortems-Cheiney, A., Pison, I., and Saunois, M.: Decadal trends in global CO emissions as seen by MOPITT, Atmospheric Chemistry and Physics, 15, 13 433–13 451, https://doi.org/10.5194/acp-15-13433-2015, https://www.atmos-chem-phys.net/15/13433/2015/, 2015.

Yin, Y., Ciais, P., Chevallier, F., van der Werf, G. R., Fanin, T., Broquet, G., Boesch, H., Cozic, A., Hauglustaine, D., Szopa, S., and Wang, Y.: Variability of fire carbon emissions in equatorial Asia and its nonlinear sensitivity to El Niño, Geophysical Research Letters, 43, 10,472–10,479, https://doi.org/10.1002/2016GL070971, 2016.

Yokelson, R. J., Andreae, M. O., and Akagi, S. K.: Pitfalls with the use of enhancement ratios or normalized excess mixing ratios measured in plumes to characterize pollution sources and aging, Atmospheric Measurement Techniques, 6, 2155–2158, https://doi.org/10.5194/amt-6-2155-2013, 2013.

Zheng, B., Chevallier, F., Ciais, P., Yin, Y., Deeter, M. N., Worden, H. M., Wang, Y., Zhang, Q., and He, K.: Rapid decline in carbon monoxide emissions and export from East Asia between years 2005 and 2016, Environmental Research Letters, 13, https://doi.org/10.1088/1748-9326/aab2b3, 2018a.

Zheng, B., Chevallier, F., Ciais, P., Yin, Y., and Wang, Y.: On the Role of the Flaming to Smoldering Transition in the Seasonal Cycle of African Fire Emissions, Geophysical Research Letters, 45, 11,998–12,007, https://doi.org/10.1029/2018GL079092, 2018b.